MASTERARBEIT / MASTER'S THESIS

Titel der Masterarbeit / Title of the Master's Thesis

„Development of a fast timing barrel scintillator hodoscope using silicon photomultipliers (SiPMs) for the $\overline{\text{P}}$ANDA experiment"

verfasst von / submitted by

Marius Constantin Chirita Mihaila, BSc.

angestrebter akademischer Grad / in partial fulfilment of the requirements for the degree of

Master of Science (MSc.)

Wien, 2017 / Vienna, 2017

Studienkennzahl lt. Studienblatt / degree programme code as it appears on the student record sheet:	A 066 876
Studienrichtung lt. Studienblatt / degree programme as it appears on the student record sheet:	Masterstudium Physik
Betreut von / Supervisor:	Prof. Dr. Eberhard Widmann

Abstract

The $\overline{\text{P}}$ANDA experiment at FAIR situated in Darmstadt, Germany will use proton-antiproton collisions, with momenta ranging from 1.5 GeV/c to 15 GeV/c, for strong interaction studies. The detector is currently under construction. It will be in operation after 2022. In order to identify the charged particles accurately, and differentiate between subsequent events, the detector will need several advanced particle identification systems.

We are working on the development of a SciTil (Scintillator Tile) hodoscope detector, which will be located in the central region (20º-140º) and cover ~5.7 m^2 area. It is built out of 1920 scintillator tiles, each of which has a dimension of 90x30x5 mm^3, and is readout by Silicon Photomultipliers (SiPM). The SciTil detector will be capable of providing fast and highly accurate event timing. The requirements for this detector are an intrinsic time resolution below σ = 100 ps and a geometry which fits along 2 cm in radial direction.

The goal of this thesis is to investigate and improve the time resolution of a single scintillator tile. After optimizing the scintillator material, sensors, wrapping etc., the best time resolution we achieved was σ~50 ps with 4 Hamamatsu SiPMs S13360-3050-PE connected in series.

2. Kurzfassung

Das $\overline{\mathrm{P}}$ANDA Experiment bei FAIR in Darmstadt, Deutschland, wird Antiproton-Proton Annihilationsprozesse bei einem Antiprotonen Impuls von 1.5 GeV/c bis 15 GeV/c verwenden, um die starke Wechselwirkung zu untersuchen. Der PANDA Detektor befindet sich derzeit im Bau und wird ab 2022 in Betrieb sein. Um die resultierenden Teilchen nach der Kollision genau zu indentifizieren und zwischen aufeinander-folgenden Ereignissen zu unterscheiden, braucht das Experiment ein fortgeschrittenes Detektorsystem für die Teilchenidentification.

Wir arbeiten an der Entwicklung und dem Bau eines Flugzeitdetektors, der SciTil (Scintillator Tile) Hodoscope Detektor, der im Zentralbereich ($20^{\circ} - 140^{\circ}$) liegt und eine Fläche von $\sim 5.7\mathrm{m}^2$ hat. Der SciTil Hodoscope Detektor wird aus 1920 Szintillatoren errichtet werden, wobei jeder Szintillator eine Dimension von $90\mathrm{x}30\mathrm{x}5\ \mathrm{mm}^3$ hat und von Silizium Photomultipliern (SiPM) ausgelesen wird. Der Detektor muss eine Zeitauflösung unter σ=100 ps haben und darf eine maximale radiale Dicke von 2 cm aufweisen.

Die Entwicklung eines einzelnen Prototypen (Szintillator+SiPMs) ist in der Endphase. Nach der Optimierung von Szintillatormaterial, Reflexionsmaterial, Sensoren etc. ist die beste gemessene Zeitauflösung σ∼50 ps, die mit 4 Hamamatsu SiPMs (S13360) in einer seriellen Verbindung erreicht wurde.

Acknowledgement

I would first like to thank to supervisor Dr. Eberhard Widmann for providing the opportunity to do my thesis at Stefan Meyer Institute (SMI), and for taking the time to make corrections to my thesis. He introduced me to the working group responsible for PANDA experiment. Research expeditions to CERN and several times in Germany were financially supported by the institute and I am very grateful for that.

I would especially like to acknowledge Dr. Ken Suzuki from SMI as the team leader of my working group. He constantly guided me and steered me in the right direction. He taught me the scientific way of thinking and encouraged me to present my research work at PANDA collaboration meetings. Without his passionate participation, I would not have been able to improve.

In particular, I would like to thank my colleague Dr. Lukas Gruber, who constantly shared his laboratory skills and expertise with me. Whenever I ran into trouble, or had a research related question, he was there giving me the answer.

Thanks to my colleague Dominik Steinschaden for helping me with computer related issues and for his moral support.

Special thanks to my colleague Aaron Capon for taking the time to make corrections to my thesis.

I would also like to thank my colleagues and friends Oswald, Julia, Peter, Mohamed, Gamal, Manfred, Markus, Andreas, Sebastian Lehner, Sebastian Zimmermann, Raluca, Darie Clitan, Octa, Sebastian Lekart, Andrea, Umar, Minja, and Victor Serban for their help and interesting discussions. Furthermore, I would like to express my gratitude to Dr. Johann Zmeskal, Dr. Johann Marton and to the technical staff: Ing. Herbert Schneider, Mark Pruckner, Doris Pristauz and Leonard Stohwasser.

I would like to take this opportunity to thank to Erlangen research group: Albert Lehmann (group leader), Merlin (master student), Fred (post doc) and Daniel (master student) for their scientific help and hospitality.

Special thanks to Mariana and Alexandru Mariutan for their overall support.

Finally, and most importantly, I must express my very profound gratitude to my parents, grandparents and brother for their love and unfailing support.

Contents

Chapter 1

1. Introduction

Fast timing and efficiency in scintillation based detectors are significant requirements for a variety of applications such as time of flight positron emission tomography (TOF-PET) or particle identification in high energy physics experiments [1, 2, 3].

The detection of low intensity light became feasible a few years after A. Einstein formulated the photoelectric effect (1905), when Elster and Geiter invented the photoelectric tube. The detection of single photons was possible after the development of photomultiplier tube (PMT) in 1936. A significant disadvantage of PMTs is that they are very sensitive to external magnetic fields. Many modern experiments in high energy physics require strong magnetic field in order to bend the charged particles and determine their momentum. For this reason, new methods of low intensity light detection have been developed. Semiconductor photodetectors like silicon photomultipliers (SiPMs), which are immune to the effects of magnetic fields, are a good candidates to replace the PMTs. Furthermore, SiPMs can be operated at low voltages, they are mechanically robust, have a good photon detection efficiency (PDE), and excellent time resolution [4, 5]. For medical applications like TOF-PET imaging a good time resolution is indispensable. The reduction of random events and precise localizing of the positron annihilation in the affected tissue leads to a conclusive diagnose [6].

The fast timing barrel scintillator hodoscope (SciTil) is a TOF detector, which is developed by the Stefan Meyer Institute in Vienna (by 90 %). The SciTil detector will be the only detector in PANDA with an excellent time resolution and is very important for event timing and particle identification. The requirements of this detector are a time resolution below 100 ps sigma and to fit in 2 cm radial direction.

The purpose of this this work is to investigate, optimize and improve the time resolution of a single scintillator tile. A detailed measurement campaign has been done in order to optimize the scintillator material, wrapping, and SiPMs with their connection and voltage amplifiers. In this context, the research has a preponderant experimental character and it implies using typical readout/front end electronics (voltage amplifiers, oscilloscope, NIM, VME modules etc.) in high energy physics.

In the following text, an introduction to the FAIR facility, PANDA experiment and its detector systems will give an overview about the physics motivation. Specially designed scintillators and SiPMs for fast timing purposes will be described afterwards. The core of this thesis (chapters 5, 6, 7) concentrates on experimental studies realized during one year at SMI and can be divided into three parts. First, the experimental setup in Vienna had its objective to understand the limiting factors of the time resolution. The second experimental setup was done under very strict laboratory conditions in Erlangen and delivered results which are being implemented in the technical data report (TDR) of the SciTil detector. The last measurement was done at CERN, where the already optimized single tile prototype was tested under a beam of high energy particles. In all three different configurations, the time resolution was well below 100 ps, and therefore the single tile was properly optimized.

Chapter 2

2. The PANDA Experiment at FAIR

The PANDA (Antiproton Annihilation in Darmstadt) experiment is currently in the planning phase and it will be operational from 2022 onwards at the Facility for Antiproton and Ion Reasearch (FAIR) in Darmstadt, Germany [7].

The PANDA detector will use proton-antiproton collisions with momenta ranging from 1.5 GeV/c to 15 GeV/c, at an average interaction rate of 20 MHz resulting in a center of mass energy range from $\sqrt{s}$= 2.5 to $\sqrt{s}$= 5.47 GeV. This will open up a large area of research, such as strong interaction studies (QCD bound states) or electroweak physics investigations (CP-violation) [8]. "The PANDA Collaboration, with more than 450 scientists from 17 countries intends to do basic research on various topics comprising hadron spectroscopy, search for exotic hadrons, hadrons in media, nucleon structure and exotic nuclei".[1]

2.1 The FAIR accelerator complex

The accelerator facility will be built at the GSI Helmholtz center for Heavy Ion Research in Darmstadt, Germany [9]. The accelerators will deliver high-intensity primary beams of protons and heavy Ions, as well as secondary beams of antiprotons with an unprecedented quality [3]. Diverse complex physics programs will run in parallel, all of them included in the four pillars: APPA (Atomic, Plasma Physics and Applications), CBM (Compressed Baryonic Matter), NUSTAR (Nuclear structure, Astrophysics and Reactions) and PANDA (Antiproton Annihilation at Darmstadt) [10]. The GSI facility uses an universal linear accelerator (UNILAC) which can accelerate ions up to Uranium. The upgraded version of GSI will include also a linear proton accelerator (LINAC), which will be operated as a pre-accelerator for the new facility. The whole FAIR complex can be seen in Fig. 2.1. The path towards proton antiproton collision is in Fig. 2.2 [10].

---

[1] http://www.scholarpedia.org/article/The_Panda_experiment

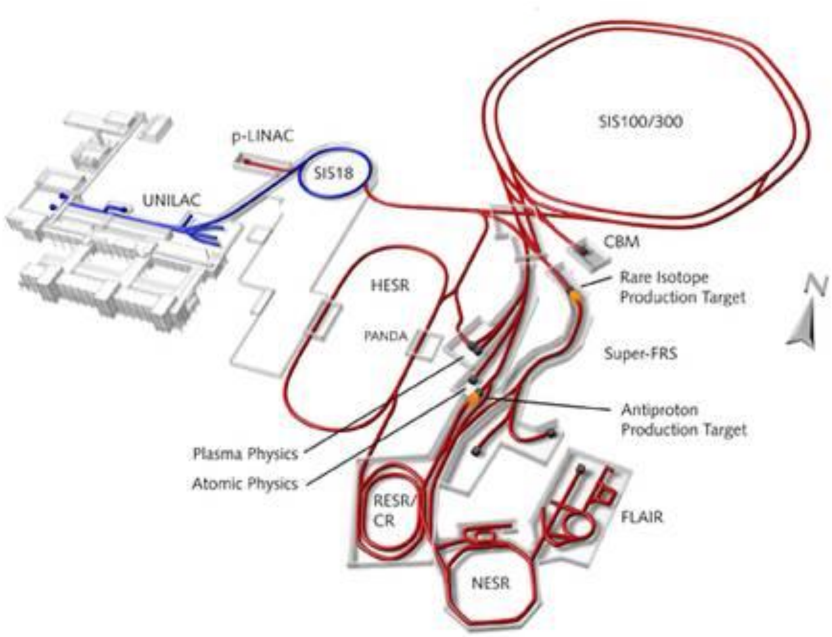

Figure 2.1: Graphic view of the FAIR accelerator complex including the 4 physics programs (APPA, CBM, NUSTAR and PANDA). The blue color shows the existing accelerators and red color stands for the new facilities, which are currently under construction. Figure taken from [10].

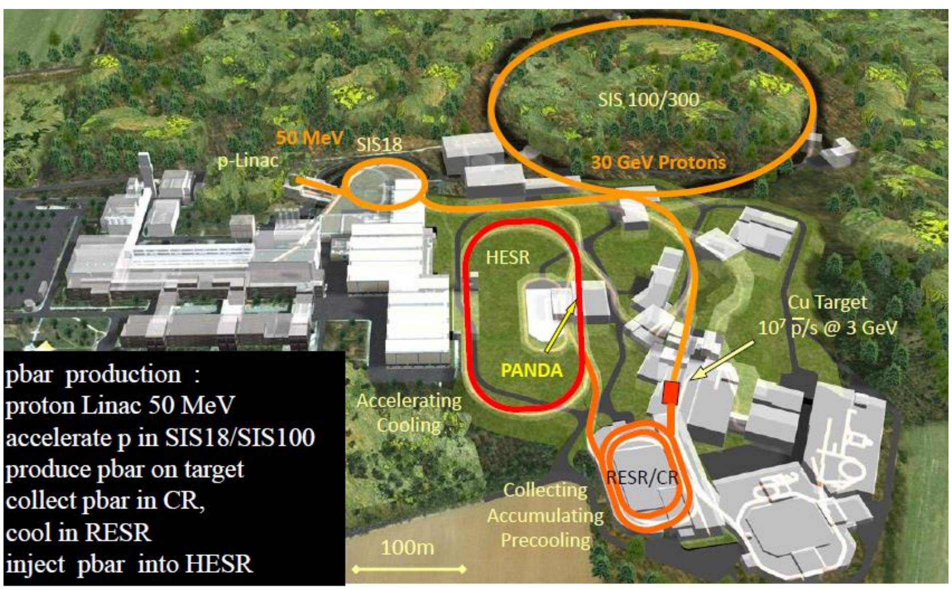

Figure 2.2: Accelerator scheme for PANDA Experiment [2].

The PANDA experiment will need antiprotons and they are produced as follows. The journey of protons (see Fig. 2.2) starts at the p-Linac where they reach an energy of 70

[2] Gianluigi Boca" PANDA at FAIR :physics goals and experimental overview" talk, Hirschegg, January 2011

MeV. For achieving higher energies they are guided towards the synchrotron SIS18 and after that they are injected into the double ring accelerator SIS100 (Heavy Ion Synchrotron, for PANDA only one ring is needed). The synchrotron has a circumference of 1100 meters and can produce high intensity proton beams (2×10^{13} protons compressed in bunches) and energies up to 30 GeV [10,11]. After acceleration, the high intensity beam of protons is impinged onto a copper/nickel target where the antiproton production takes place. The resulting beam of antiprotons (at least 1×10^{8}) will be collected in the collector ring and transferred in single bunches to the RESR (Accumulator Storage Ring) where stochastic cooling is applied. The prepared antiprotons with a momentum of 3.8 GeV/c will then be injected in the High Energy Storage Ring (HESR), where they can circulate for up to several days. The beam of antiprotons can be accelerated or decelerated within a range of 1.5 to 15 GeV/c and will collide on a fixed proton target. Up to 10^{11} antiprotons can be stored in HESR. The storage ring requires a proficient cooling system (electron cooling and stochastig cooling) in order to maintain the expected performance [12].

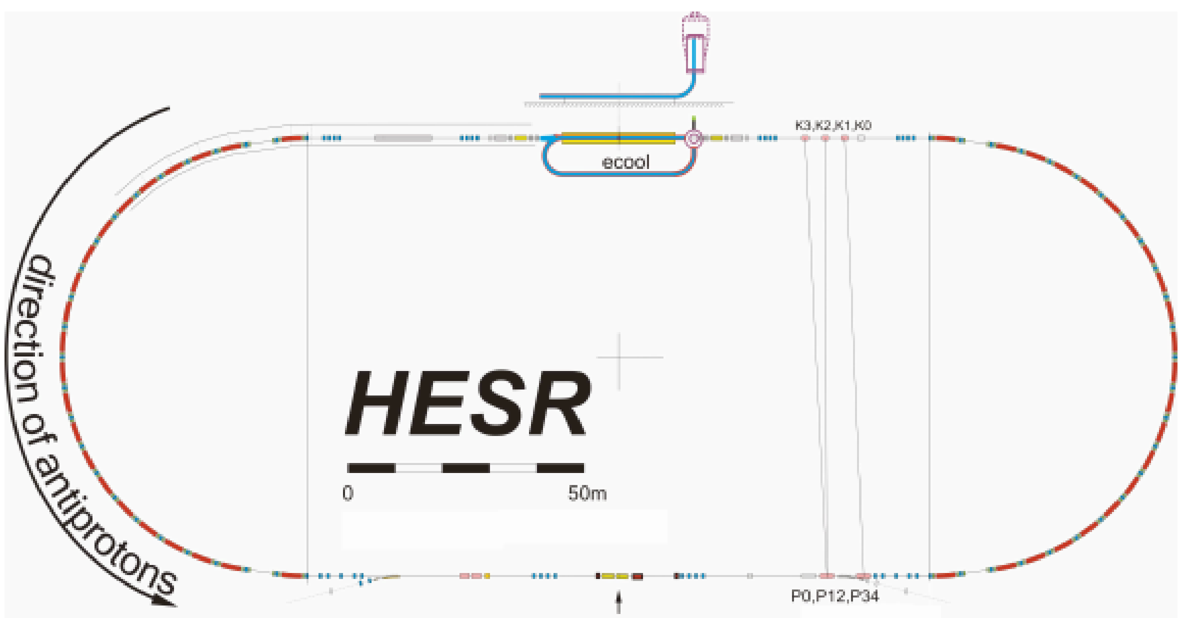

Figure 2.3: Schematic of the HESR adapted from [12]. Cooling systems and injection position of antiprotons indicated.

The design of the HESR will have on one side the cooling system and on the other side the experimental installation of the PANDA detector with target system. Two operation modes are being envisaged for the PANDA experiment: a high luminosity mode (HL), reaching a luminosity up to $2 \cdot 10^{32} \cdot cm^{-2} \cdot s^{-1}$, and a high resolution mode (HR), with a momentum resolution of $\Delta p/p \leq 10^{-5}$[13]. Table 2.1 lists the information about the two operation modes.

	High luminosity mode	High resolution mode
Momentum [GeV/c]	1.5 –8.9	1.5 –15
Number of antiprotons	10^{11}	10^{10}
Momentum spread $\Delta p/p$ (rms)	$\Delta p/p \leq 10^{-4}$	$\Delta p/p \leq 10^{-5}$
Peak luminosity [$cm^{-2} \cdot s^{-1}$]	$2 \cdot 10^{32}$	$2 \cdot 10^{31}$
Beam cooler	Electron ≤ 8.9 GeV/c	Stochastic ≥ 3.8 GeV/c

Table 2.1: HESR operation mode. Values adapted from [11].

2.2. PANDA Physics research goals

A brief description of the physics goals at PANDA will follow. Complete information about this subject can be found in the PANDA physics book [9].

Hadrons are bound states of QCD, the theory which is describes the strong interaction. The strong force acts between quarks. The mediating particles that facilitate the strong force are gluons. The quarks are imprisoned inside hadrons and this is called in physics the quark confinement. No matter how hard one tries to separate them, quarks have never been observed isolated. Until this point there is no analytical theory, which can fully explain this phenomena [14].

Major physics topics will be investigated as follows:

QCD bound states in the range of 2.45-5.47 GeV: High precision Charmonium spectroscopy; open and hidden charm states; exotic states like hybrids, glueballs, oddballs, and multiquarks which are predicted by the QCD and are more likely to be found in this mass range (3-5 GeV/c^2). Non perturbative QCD dynamics in baryons: measure $p\bar{p} \rightarrow \Lambda_c \overline{\Lambda_c}$ with high statistics at a momentum above 2 GeV/c. Hypernuclear physics: the high luminosity will make it possible to study hyperon-nucleon and hyperon-hyperon interactions. Electroweak physics: CP violation in charm mesons and baryons, and forbidden decays will be investigated. [11, 12].

2.3. PANDA detectors

The experiment should have a good particle identification system, high tracking resolution in a strong magnetic field and calorimetry with high energy resolution for detecting charged particles and photons. The data acquisition should be continuous and the trigger system efficient. The PANDA detector is divided into the target spectrometer (TS) and forward spectrometer (FS) [12]. The target spectrometer consists of a solenoid situated around the interaction region which generates a highly homogeneous magnetic field of 2 T. The subdetectors within the solenoid are installed in onion like layers. The forward spectrometer consists of a dipole magnet (1T) and its afferent detectors in order to analyze the momentum of forward going particles [12, 13]. Fig. 2.5 shows the PANDA detector with the target, tracking and PID systems, as well as the electromagnetic calorimeter [9, 13]:

The **target System** consists of either frozen hydrogen microspheres (pellets) or clusters of nano-particles (cluster jets).

The **tracking system** will run under the influence of two different magnetic fields (depending if it is in TS or FS) and will measure the flying path of charged particles:

The Micro Vertex (MVD) Detector is located in the TS and is closest to the interaction point. It is build out of granular silicon pixel detectors or double sided silicon strip detectors. It is specially designed to detect short-lived charged particles.

The Central Tracking (CT) Detector should have a momentum resolution of $\Delta p/p \sim$1-2 %. For this, a straw tube tracking system (STT) is being considered. PID information can also be extracted.

The Gas Electron Multiplier (GEM) station will be the first forward tracking detector after the CT. The position resolution will be $\text{better than } 100\ \mu\text{m}$.

The forward mini drift chamber system is designed to track deflected particles in the forward direction.

The **PID system** should identify the charged particles accurately and therefore the following subdetectors are being considered: Detection of Internally Reflected Cherenkov light (DIRC), Time of Flight (TOF) counter, Muon Detection (MD) system and Ring Imaging Cherenkov (RICH) detector. Together with positional information from the tracking system and energy information from the EMC, a complete identification profile will be possible.

The electromagnetic calorimeter will consist of many small inorganic scintillators ($PbWO_4$) readout by Avalanche Photo Diodes (APD). The goal of the calorimeter will be to have a high energy resolution for detecting photons and charged particles (mostly electrons).

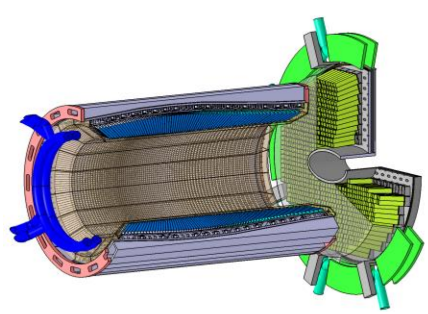

Figure 2.4: Electromagnetic calorimeter with its barrel and forward cap. Adapted from [12]

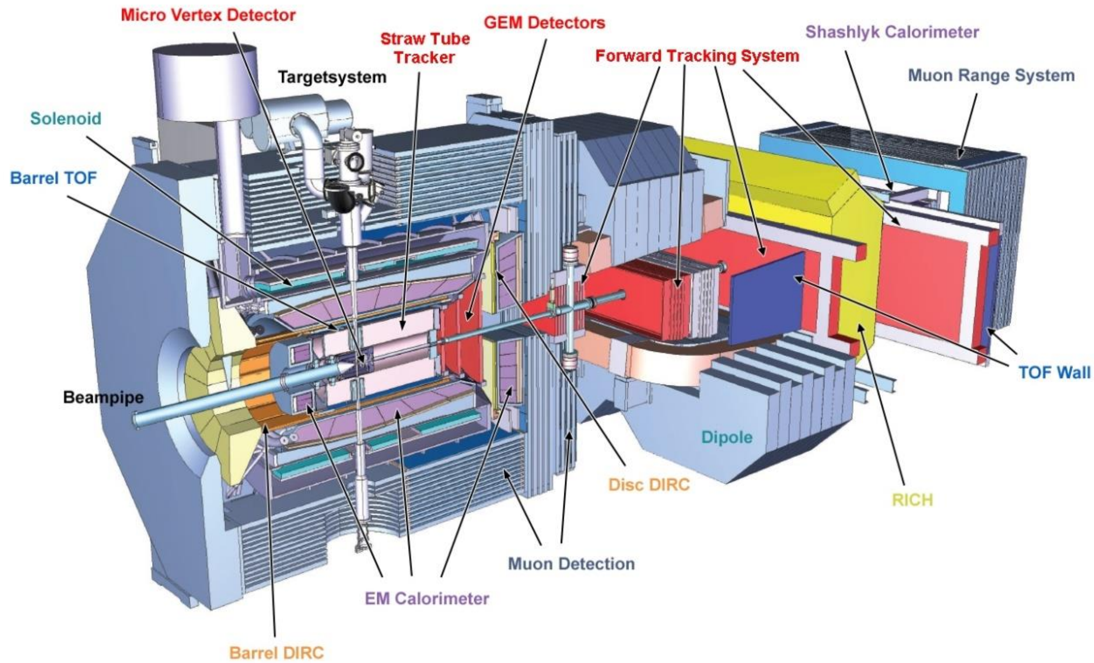

Figure 2.5: 3D picture of the whole detector system. Figure adapted from [10]

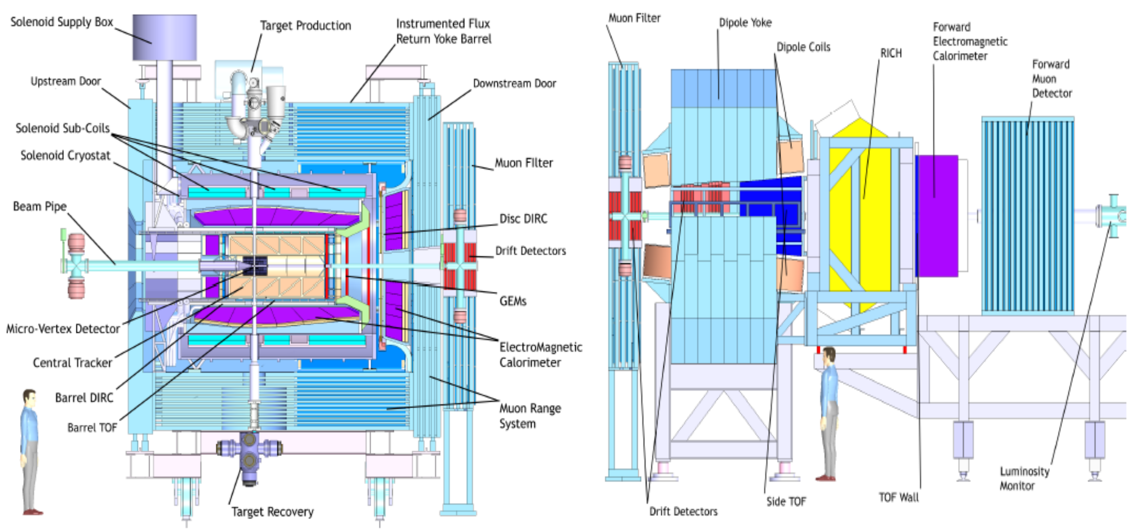

Figure 2.6: Side view of the target- (left) and forward spectrometer (right). Figure adapted from [12].

A detailed description of the PANDA detector system can be found in [9].

Chapter 3

3. The barrel TOF (SciTil) detector

The TOF (alias SciTil) detector is a barrel-shaped detector located in the center of the target spectrometer covering a polar angle of 20° to 140°. The barrel is 180 cm long and covers an area of about 5.7 m^2[7]. The SciTil will be composed out of 1920 scintillator tiles divided into 16 supermodules in azimuthal direction. The neighboring detectors of the SciTil are barrel DIRC (inwards) and EMC (outwards) in radial direction.

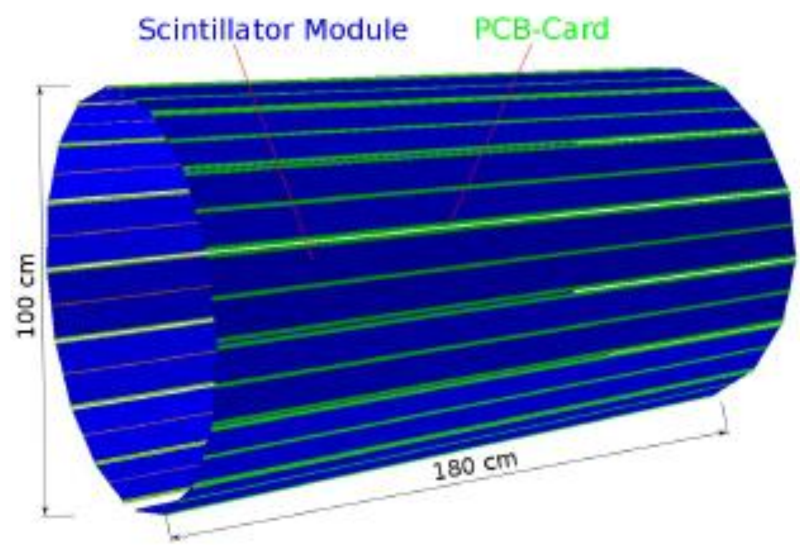

Figure 3.1: Design of the SciTil detector with its 16 super-modules containing 1920 scintillator tiles, 15360 SiPMs and 3840 channels. Figure adapted from [15].

The detector operates under the following principle: incident particles will pass through the scintillator material depositing energy. The lost energy in the scintillator will generate fluorescent photons, which are being detected by the SiPMs and converted into an electric signal. Since it is a TOF, the scintillators, SiPMs and readout electronic should be specially designed for fast timing applications. Each scintillator tile is readout on the left and right side by 4 SiPMs connected in series (see Fig. 3.2). Following figures will show the design concept of the SciTil detector.

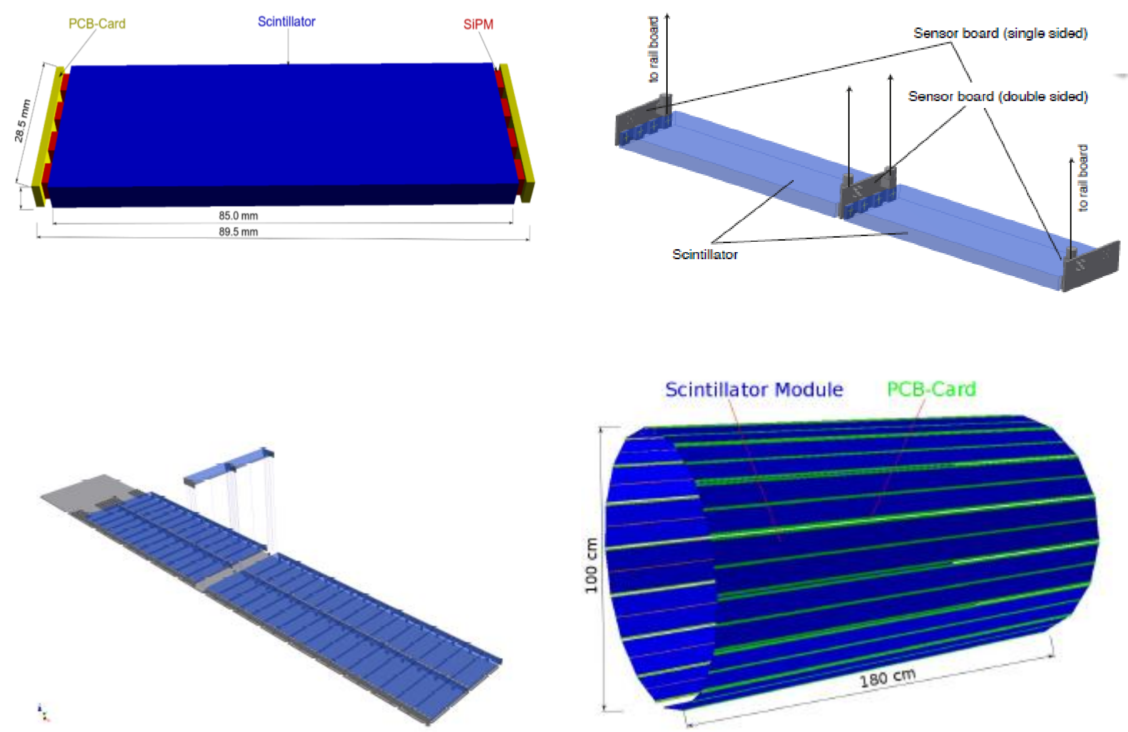

Figure 3.2: From a single tile to the complete SciTil detector. The SciTil Hodoscope (bottom right) is made out of 16 super-modules (bottom left), and each super-module contains 60 dual modules (bottom right). The dual module (top right) is made out of two single scintillator tiles with a double sided sensor board in the middle in order to maximize the efficiency of the detector. The single tile is shown top left and is composed out of a scintillator that is readout by 4 SiPMs on each side.

The SciTil detector will have a good mechanical shock resistance and should be able to operate over a period of 10 years. The main capabilities of the SciTil are: particle identification (for low momentum particles, below ~700 MeV/c, at large polar angles), event sorting, pattern matching/track seeding and EMC preshower detection. A TOF detector can differentiate between particles which have the same momentum, but different mass. The SciTil detector is not a standard TOF detector, since a TOF detector requires a two stage scintillation detection (start and stop signal). Nevertheless, a fast timing counter in the target spectrometer improves significantly the overall performance of the PANDA detector. A full description of the SciTil detector can be found in the technical data report (TDR) [15].

In order to achieve the physics goals of the PANDA experiment, the SciTil detector requires a time resolution under σ=100 ps. Since the whole detector is made out of many single tiles, a major step towards reaching this goal is to optimize the time-resolution of a single tile (scintillator+4 SiPMs on each side) and this is the purpose of this thesis.

3.1 Scintillator material

Two different scintillators are being considered: EJ-232, EJ-228

Properties	EJ-228	EJ-232	EJ-232Q 0.5% BP	EJ-232Q 1% BP
Scintillation Efficiency (photons/1MeV e^-)	10200	8400	2900	1700
Light Attenuation Length (cm)	-	10	10	10
Rise Time (ns)	0.5	0.35	0.110	0.105
Decay Time (ns)	1.4	1.6	1.6	0.7
Wavelength of Maximum Emission (nm)	391	370	370	370
Pulse Width, FWHM (ns)	1.2	1.3	1.3	0.29
Denisity (g/cm^3)	1.023	1.023	1.023	1.023

Table 3.1: Scintillator properties of fast timing scintillators EJ-228, EJ-232, as well as the quenched version, EJ-232Q, which is doped with Benzophenone (BP) Atoms to reduce the rise and decay time. Values taken from the data sheets of Eljen Technology [3].

At the moment, EJ-228 and EJ-232 are among the fastest plastic scintillators on the market. The significant properties of a scintillator used for fast timing applications are a high light yield (scintillation efficiency) and short rise/decay time. For the following measurements (in Chapter 5), these two scintillators were tested. In order to maximize the efficiency, the wavelength of maximum emission of the scintillator should match the peak sensitivity wavelength of the readout SiPMs.

[3] http://www.eljentechnology.com/index.php/products/plastic-scintillators

Recently, Eljen Technology developed an "ultrafast" scintillator, which is the quenched version of EJ-232. The values from data sheet (see Table 3.1) indicate, that the rise/decay time improves, but the light yield decreases. Past experience has shown that the signal rise/decay time is a key component in fast timing, but so is high light yield. In the near future, a test with the new quenched scintillator is envisaged, to see if the time resolution of the prototype improves.

3.2. Time resolution calculation, the "L-R method"

Assuming the measurement setup in Fig. 3.3, the timing of the scintillator counter (scintillator+sensors) $t_{counter}$ is defined as [16]:

$$t_{counter} = \frac{1}{2} \cdot (t_L + t_R) = f \tag{3.1}$$

with t_L and t_R being the output signal time from left and right sensors. The time resolution of the counter is given by following expression:

$$\Delta t_{counter} = \sqrt{(\frac{\partial f}{\partial t_L})^2 \cdot \Delta {t_L}^2 + (\frac{\partial f}{\partial t_R})^2 \cdot \Delta {t_L}^2} \rightarrow$$

$$\Delta t_{counter} = \frac{1}{2} \cdot \sqrt{\Delta {t_L}^2 + \Delta {t_R}^2} \tag{3.2}$$

If there is a counter and an incoming beam of collimated charged particles (see Fig. 3.3), the only way to measure the time resolution of the counter is by calculating the time difference between left (L) and right (R) sensors [3].

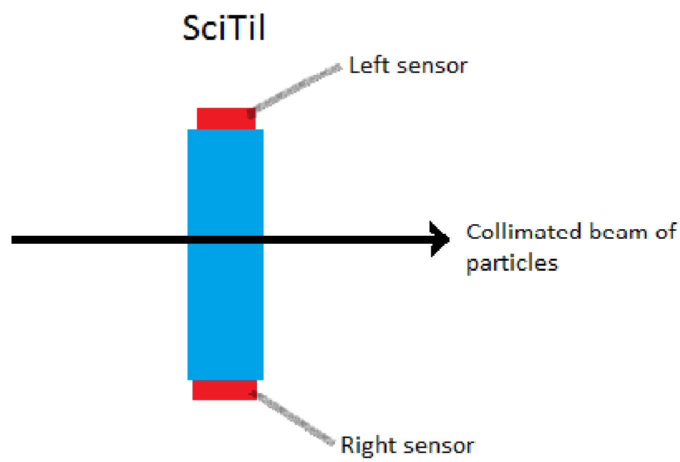

Figure 3.3: Schematic of a measurement setup for calculating the time resolution of the counter which consists of a scintillator (blue) and two sensors (L and R, red).

Ignoring the flight path through the scintillator volume, the TOF between L and R sensor is given by the following expression:

$$TOF_{L-R} = t_L - t_R = f(t_L, t_R) \qquad (3.3)$$

Of course the $\mathrm{TOF_{L-R}}$ will not always be the same, so that the amount of variation will be given by the standard deviation of the data values. From equation (3.3) it follows:

$$\Delta TOF_{L-R} = \sqrt{(\frac{\partial f}{\partial t_L})^2 \cdot \Delta t_L{}^2 + (\frac{\partial f}{\partial t_R})^2 \cdot \Delta t_R{}^2} \rightarrow$$

$$\Delta TOF_{L-R} = \sqrt{\Delta t_L{}^2 + \Delta t_R{}^2} \qquad (3.4)$$

Combining (3.2) and (3.4) the time resolution of the scintillator counter can be given by the following equation [16]:

$$\Delta \boldsymbol{t}_{\boldsymbol{counter}} = \frac{\boldsymbol{\Delta TOF_{L-R}}}{\boldsymbol{2}} \quad \textbf{(σ of the detector)} \qquad (3.5)$$

This way of calculating the time resolution was used in the laboratory measurements of chapter 5 and 6. There are also other ways to calculate the time resolution of a counter when multiple detectors are involved (see [17]).

Chapter 4

Silicon photomultiplier

Silicon photomultipliers (SiPMs) are used to detect low intensity light down to the single photon level. Their capability of detecting low light signals is similar to that of a PMT, while having the advantage of a solid-state device (robustness, insensivity to magnetic field, low voltage operation etc.). A SiPM device consists primarily of multiple avalanche photodiodes (APD) connected in parallel and operating in Geiger-mode. They are also known as Multi-Pixel-Photon Counter (MPPC), where each pixel is a series connection between a APD and a quenching resistor R_q[18, 19].

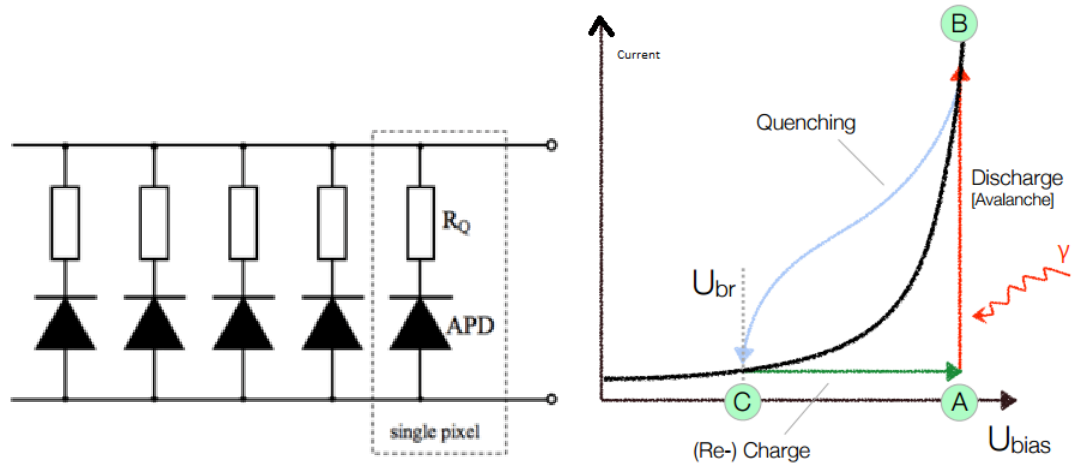

Figure 4.1: A single pixel consisting of serial connection between APD and R_q, while the pixels are connected in parallel (left). The right figure shows the working cycle of a photodiode operating in Geiger-mode. There are 3 stages. Apply a bias voltage above the breakdown voltage, so that the created charge carrier from an absorbed photon, or thermal noise, will generate an avalanche. The pixel capacitance starts to discharge and causes a voltage drop across R_q, after which quenching occurs and the diode returns to its initial state. Figures adapted from [19, 20, respectively].

When a single photon (hv) hits the APD, an e-h (electron-hole) pair can be created if the energy of the photon is greater than the band gap energy (E_g) of the APD (typically 1.1 eV in silicon). Due to the applied reverse bias (ranging from 30 to 70 V), a high electric field is created in the depletion region of the diode, which separates the created electron hole pair. The electric field is so high that the primary created electron (or hole) generates further ionization by creating an avalanche. An avalanche can produce up to $10^5 - 10^6$ e-h pairs and their drift towards the electrodes will induce a current that can be measured. In order to stop this avalanche in the APD, and in order to prepare the sensor for the “next photon”, a passive-quenching resistor is connected in series with the APD. Once an upper current limit is reached during the breakdown of the APD, the resistor will quench it and the reverse voltage will drop slightly below the breakdown voltage. The operation circle of an APD is shown in Fig. 4.1. Now, there is the question of what happens if two or more photons hit a single APD at the same time? Is the resulting signal proportionally higher? The answer is no. The resulting signal has the same amplitude and duration as when only a single photon is absorbed (Geiger-mode). The SiPM is therefore made out of multiple APDs connected in parallel, so that if distinct APDs simultaneously absorb photons, the resulting amplitude will be proportional to the number of independently triggered APDs [18,21,22].

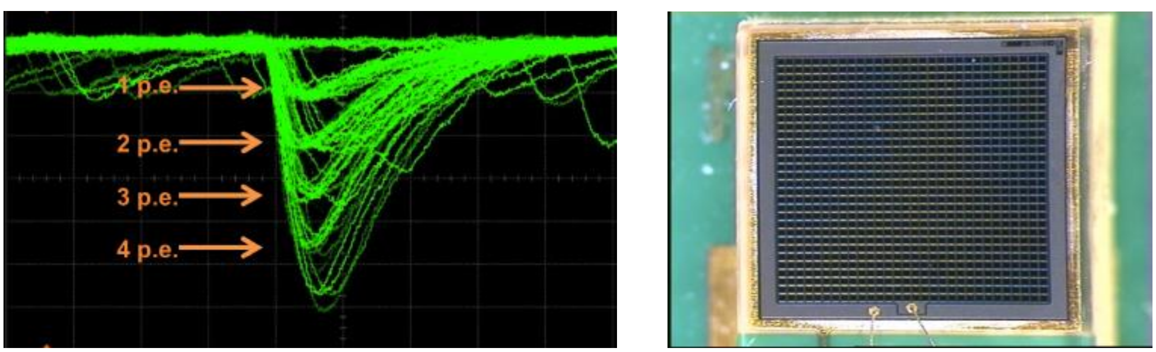

Figure 4.2: A typical pulse shape of a SiPM showing the proportionality between number of independently triggered APDs and pulse amplitude (left). For example 3 p.e. (photo-electrons) means that at the same time 3 independently APDs were triggered (Figure adapted from [18]). The picture in the right is showing a typical SiPM with its single pixels containing a multitude of APDs (Picture taken by G. Ahmed with a light microscope).

4.1. Properties of a SiPM

The SiPM is reverse biased with a voltage value that is slightly above the breakdown voltage (V_{br}). This over voltage ($\Delta V = V_{bias} - V_{br}$) is a decisive parameter, because it controls the detector performance. The breakdown voltage of a SiPM marks the moment when the generated electric field is high enough to produce a Geiger discharge. At this point, an immediate increase of current is observed. A high quality SiPM should have the following properties: high gain and photon detection efficiency (PDE), as well as low dark counts rate, afterpulsing and optical crosstalk [18].

4.1.1. Gain

The gain of the SiPM refers to the produced charge by a single APD during an avalanche. The gain (G) is a function of pixel output capacitance (C_{pix}) and over-voltage (ΔV), as follows,

$$G = \frac{C_{pix}}{q_e} \cdot \Delta V \qquad (4.1)$$

with q_e being the elementary charge. The capacitance value depends on the pixel size ranging from 10 fF to a few 100 fF [4]. The terminal capacitance for a 3x3 mm^2 SiPM is about 300 pF, which consists of the sum of all pixels- and other stray capacitances. A typical PMT has an output capacitance of 3 to 10 pF, which means that amplifiers used for PMTs do not perform as good for SiPMs [32]. Nevertheless the gain of a SiPM ($10^5 - 10^6$) is similar to that of a PMT.

4.1.2. Photon Detection Efficiency

The PDE gives the probability that an incident photon that hits the SiPM will create a Geiger discharge in one of the SiPM pixels. The PDE ranges from 20 to 50 % and is given by:

$$PDE(\lambda, V) = n(\lambda) \cdot \varepsilon(V) \cdot F \qquad (4.2)$$

with $n(\lambda)$ being the quantum efficiency of silicon, $\varepsilon(V)$ avalanche probability and F the fill factor of the device. The SiPM quantum efficiency depends on the wavelength of the incident photon. Due to the fact that a SiPM has a large pixelated area with small gaps between pixels, the fill factors give the ratio between active and inactive area. In general, the bigger the pixel size, the higher the fill factor. The PDE is calculated from the detector photosensitivity P and is expressed by this equation [18, 23]:

$$PDE = \frac{P \cdot h \cdot c}{G \cdot \lambda \cdot e} \tag{4.3}$$

with G the gain of the pixel, h the plank constant, c the speed of light, λ the wavelength of the incident photon, e the elementary charge and P the photosensitivity which is given by the following equation:

$$P = I_{SiPM}/I_p \quad \text{[A/W]} \tag{4.4}$$

with I_{SiPM} the measured current level and I_p the incident light power on the SiPM. From eq. 4.3 one can see that the photosensitivity is proportional to the gain, which leads to the conclusion that the lower the over voltage, the lower the photosensitivity [18, 23].

4.1.3. Noise in SiPMs

A poor signal to noise ratio significantly reduces the timing performance of the the SiPM. Three significant sources of noise are present in SiPMs: dark counts, optical crosstalk and afterpulsing effects. The primary source of noise in SiPMs is thermally generated dark counts. When the electric field in the depletion zone of the APD is high enough, a thermally generated carrier (electron or hole) can trigger an avalanche resulting in a signal pulse of one photo electron (p.e). The resulting output signal pulse does not differ from the photon generated signal pulse, therefore one should always put a minimum threshold above 1 p.e when taking data with SiPMs. The occurance of dark counts is random in time and the rate depends on several factors like: overvoltage, temperature, temperature variation and the quality of the photosensor [21].

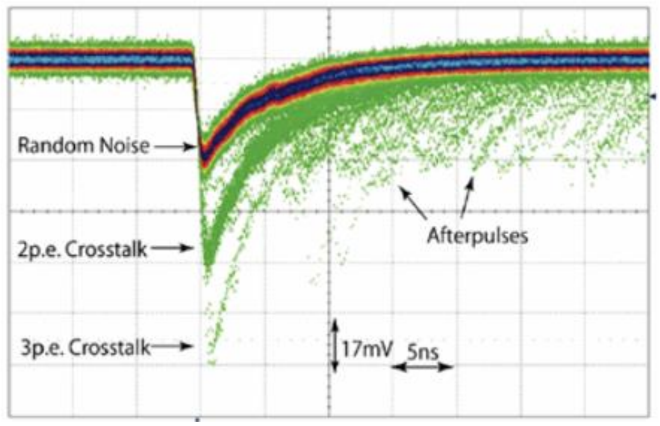

Figure 4.3: Oscilloscope screenshot showing the sources of noise present in SiPM output signal. Random dark counts, optical crosstalk and afterpulses. Figure adapted from [19].

Optical crosstalk can occur in the following circumstance; An incident photon will generate an avalanche in a pixel. During the avalanche in the pixel, additional photons can be generated and, if they have enough energy to reach neighboring pixels, they can produce an e-h pair there and initiate a correlated avalanche. Nevertheless, most of the generated photon in the pixel during an avalanche will be reabsorbed in the same pixel. This effect can be visualized in the following figure.

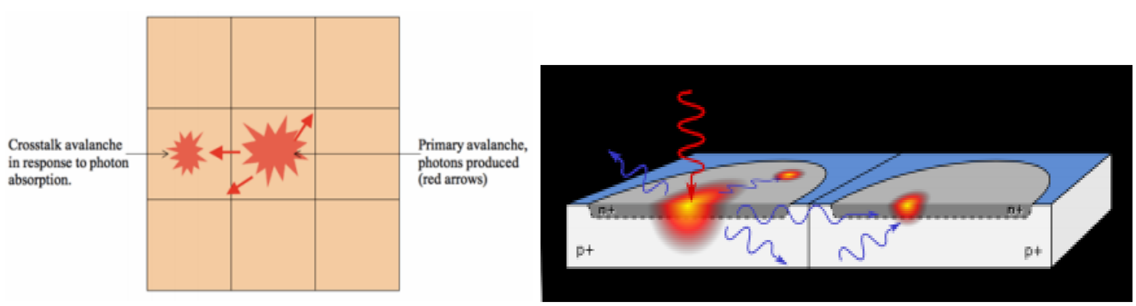

Figure 4.4: Optical crosstalk mechanism. In the left figure 9 pixels are being shown. A primary avalanche in the central pixel can produce photons with a high enough energy to reach neighboring pixels and initiate there an avalanche. The probability of induced inter pixel crosstalk decreases with the fill factor (reabsorption of photons in the same pixel). Left Fig. adapted from [21] and right figure from [20]. Some SiPMs have trenches (optical isolation) between pixels in order to undermine the crosstalk effect.

Afterpulsing occurs when some charge carriers get trapped in the primary avalanche region and are released during the recovery time of the pixel. This delayed release of trapped charge can trigger another avalanche, resulting in a so called “afterpulsing” that increases the recovery time of the fired pixel. This effect can lead to a degradation of time resolution. The probability of afterpulsing increaseswith the strength of electric field induced by a higher overvoltage [21, 23, 24].

4.1.4. Dynamic range of a SiPM

A SiPM consists of N number of pixels and its dynamic range is determined by it. Each pixel can be triggered or not, depending if the created e-h pair from absorbed photon (or dark count) induces an avalanche. The maximum output signal amplitude N p.e. is therefore reached, when all N pixels are fired at the same time. The number of triggered pixels (N_t) in response to the total number of incident photons (N_γ) hitting the SiPM area is expressed in the following formula [23]:

$$N_t = N \cdot (1 - exp(-N_\gamma \cdot PDE/N)) \quad (4.5)$$

The SiPM saturates if the number of incident photons, with respect to the flux rate increases too much. A detailed measurement of how different SiPMs respond to pulses of light can be found in [25].

4.2. S13360 series SiPMs

The time interval between the arrival time of a photon on the surface of the pixel and the moment when the pixel produces an output signal fluctuates. The rms (square root of the mean square) of this fluctuation is called time resolution (or time jitter). Since the SciTil detector is a timing counter, dedicated SiPMs with an excellent time resolution should be chosen to readout the scintillators. Compared with a typical PMT, the pulse shape of a SiPM has a much longer tail, mainly because of the avalanche effect, high pixel capacitance and passive quenching (the fired pixels need to recover between subsequent events)[37]. The new S13360 series of SiPMs from Hamamatsu have improved properties compared to previous products. That is, excellent time jitter;

reduced crosstalk, afterpulses and dark counts; better photon counting capability, as well as a lower required bias voltage [19].

For the time resolution measurements in chapter 5, two SiPM types from the S13360 series were tested. Their properties are listed in the following table:

Properties	**S13360-3050PE**	**S13360-3025PE**
Effective photosensitive area	3x3 mm	3x3 mm
Pixel pitch	50 µm	25 µm
Number of pixels	3600	14400
Number of channels	1 ch	1 ch
Spectral response range	320 to 900 nm	320 to 900 nm
Peak sensitivity wavelength	450 nm	450 nm
Dark count (typical value)	500 kcps	400 kcps
Terminal capacitance	320 pF	320 pF
Gain	$1.7 \cdot 10^6$	$7 \cdot 10^5$
Breakdown voltage (V_{br})	$\sim 52\ V$	$\sim 52\ V$

Table 4.1: Properties of S13360-3025PE and S13360-3050PE SiPMs. With kcps being kilo counts per second. Values taken from the data sheet[4].

Unlike other low intensity light detectors, SiPMs can be substantially optimized for a specific purpose from the manufacturing point to the operation point. Usually compromises have to be made in order to fulfill a specific requirement. For example the PDE increases with overvoltage, but so does the dark count rate [26]. A first time resolution test will be presented in the following chapter.

[4] Hamamatsu MPPC, http://www.hamamatsu.com/resources/pdf/ssd/s13360_series_kapd1052e.pdf

Chapter 5

5. Measurements in Vienna, laboratory tests

5.1. SiPMs connection

The goal is to have a fast output signal. Therefore, three types of connections between SiPMs are considered: the parallel, the serial and the hybrid connection. In this section the advantages and disadvantages of these connections will be presented.

The serial connection of SiPMs:

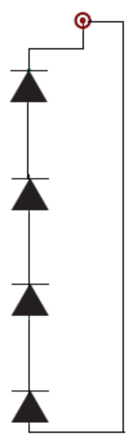

Figure 5.1: serial connection

Figure 5.2: serial connection of (KETEK) SiPMs

Serially connected SiPMs were used for the first time in [27]. The large active area of the SiPM will produce a high output capacitance, which will generate a long and slow waveform. By adding more SiPMs in series, the total capacitance of the sensors will decrease, the rise time becomes faster and the signal becomes narrower (see Fig. 5.7). An other advantage of this type of connection, in comparison with the more standard parallel connection, is the automatic adjustment of over voltage to each sensor. The downside of the serial conenction is the fact that it requiers higher bias voltage and the pulse height is reduced [28, 29].

Connecting the SiPMs in parallel has the advantage of requiring a lower bias voltage. The potential on the surface of SiPMs will be the same. On the other hand the resultant pulse shape becomes wider and slower (see Fig. 5.9).

The parallel connection of the SiPMs:

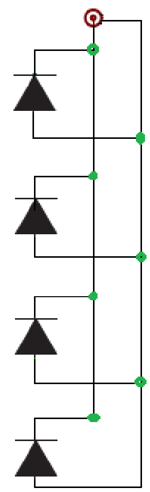

Figure 5.3: parallel connection of the SiPM, with signal line and bias line in parallel

The hybrid connection of the SiPMs:

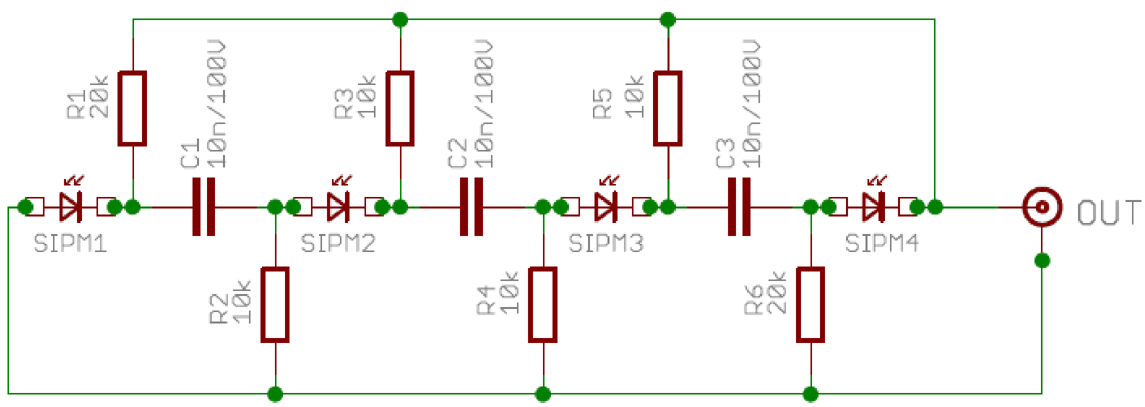

Figure 5.4: Hybrid connection of the SiPM (H. Schneider). By inserting a high pass filter between the SiPMs, the bias voltage is applied in parallel and the fast signal line is in series.

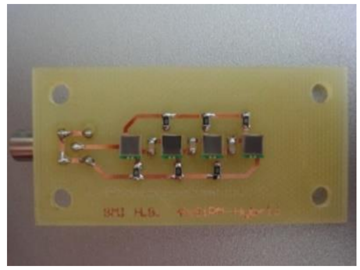

Figure 5.5: A picture of the PCB board with HAMAMATSU SiPMs in hybrid configuration (made by H.Schneider).

The hybrid connection is a mixture of serial and parallel connection. The bias line is connected in parallel while the signal line in series. The direct current coming from the bias line cannot pass through capacitators, while the high frequency signals can. This high pass filter consisting of capacitators and resistance allows the signal to be connected in series and at the same time to have a common bias voltage [28]. As a readout electronic for the SiPMs, we would like to integrate the TOF-PET chip. This TOF-PET chip might not be able to provide sufficient bias for the pure serial connection. Therefore, the hybrid connection could be an option.

5.2. Signal rise time dependency on the number of SiPMs connected in series

The signal shape of the serial connection should be analysed in order to find the best configuration that will deliver the best time resolution. A significant factor in this matter is the rise time of the signal, which should be as short as possible. The SiPMs (KETEK PM3350) were illuminated with a pulsed laser (30 ps width) and the resulting output waveform was analysed with an oscilloscope (LeCroy Waverunner 635zi, see Fig 5.10). The bias of the SiPMs was provided through the preamplifier board (photonique AMP-0611, see Fig 5.6), which was used to amplify and shape the signal. A diffuser was used to spread the laser light homogeneously across the SiPMs surface. The pulseheight drops if more sensors are connected in series. Therefore, if one wants to keep the pulseheight constant, the intensity power of the laser should be increased. The frequency of the laser was set to 1 kHz and the intesity varied from 5 to 90% of its maximum power in order to always have the same pulseheight .A PC with Labview was used to control the measurement and to record the waveforms from the oscilloscope (see Fig. 5.10).

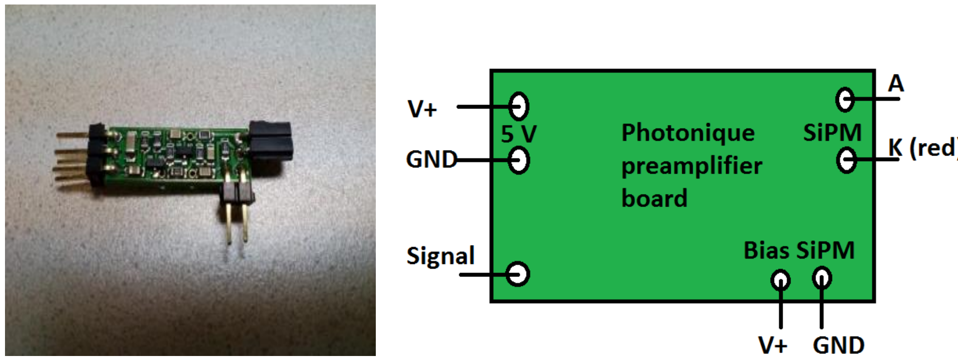

Figure 5.6: Photonique preamplifier board (left) and the layout showing how to bias the SiPMs and extract the signal. The bias voltage for the preamplifier is 5 V.

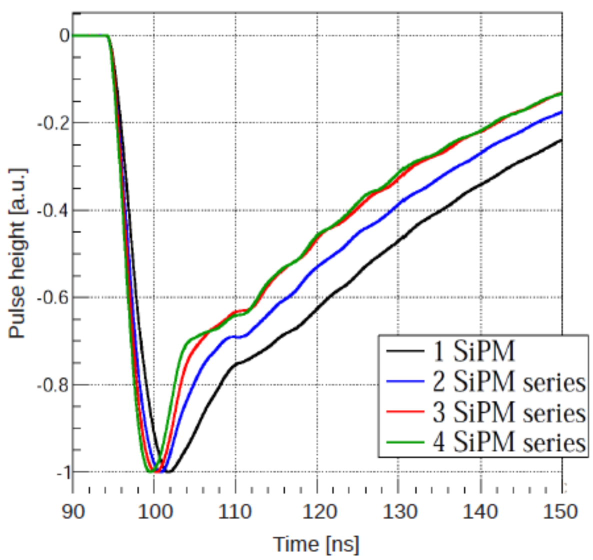

	Signal Rise Time [ns]	Width [ns] at 50% lvl
1 SiPM	4.6	30.6
2 SiPM	3.875	25.375
3 SiPM	3.375	21.875
4 SiPM	3.125	21.85

Figure 5.7: Signal rise time and width of different sensors configuration (from single sensor to 4 sensors connected in series). Figure adapted from [31].

Figure 5.7 shows a comparison between different SiPM connections. The waveforms have been normalized by their amplitudes after recording 1000 events. The values listed in Fig 5.7 show that when there are 4 SiPMs connected in series the signal rise time is about 32% shorter and its width is 30% smaller than that of a single SiPM. How much is the pulse height being reduced and is the single p.e. peak still visible when using serial connection (see Fig. 5.8)? A measurement has been done in order to see by what percent is the pulseheight being reduced when 4 SiPMs connect in series.

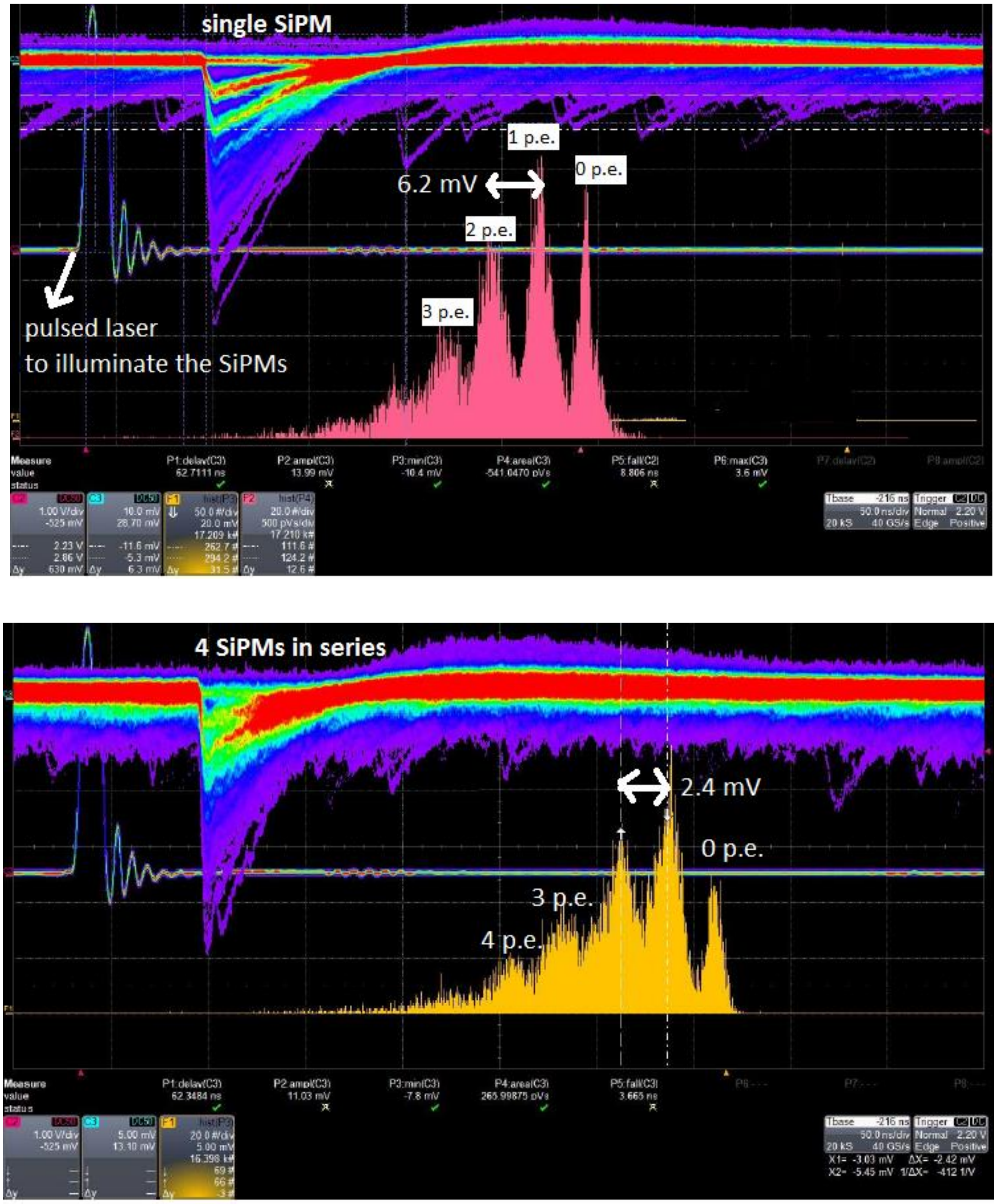

Figure 5.8: Single photo electron (p.e.) peak distribution. Pulse shape resulting from a single SiPM @ 29 bias voltage (top) and for four SiPMs in series @ 116 V(bottom, more noise). The pulseheight of a p.e. dropps by ~ 61%. Also an increase of noise is noticed.

Fig. 5.8 contains screenshots from the oscilloscope. Due to the noise and dark counts the peaks do not have a very good resolution, however the data can still be evaluated.

The upper line represents the signal coming from the SiPMs and the middle one is the pulsed laser signal, which acts as a trigger signal for the SiPMs. The single peaks from the yellow/pink histograms correspond to a fixed number of fired pixels (single photo electrons). The distance between two photo peaks shows the correlation between pulse height and photo-electrons. By using a single SiPM, one photo electron coresponds to 6.2 mV and by connecting 4 SiPMs in series, one photo electron has about 2.4 mV pulse height. The measurement from above indicates that connecting SiPMs in series will decrease the pulseheight. Nevertheless, the single photons are still visible and the photon counting capability remains. An interesting and detailed measurement with different connection types can be found in [29].

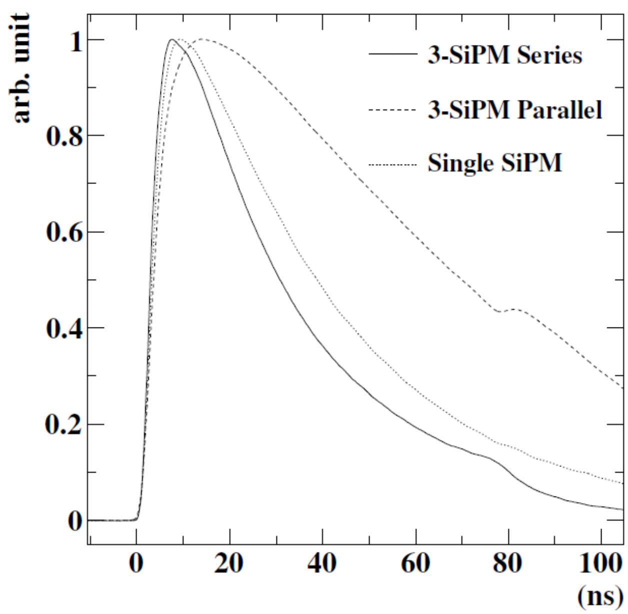

Figure 5.9: Pulse shape comparison for different SiPM connections. Scintillation signals of BC422 with HPK SiPM (S10362-33-050C) readout without the analog pulse shaping are shown. These pulse shapes are made by averaging a few thousand events and normalized by their amplitudes. Bumps at around 80 ns are due to a reflection in the readout circuit[5].

In the paper mentioned before [29], the output signal coming from a single SiPM, three SiPMs connected in series and three SiPMs connected in parallel were analysed (see Fig.

[5] Paolo W. Cattaneo a.o "Development of High Precision Timing Counter based on Plastic Scintillator with SiPM Readout" IEEE Trans. Nucl. Sci. 61, 2657-2666 (2014)

5.9). When using a serial connection, the results indicate, that the pulse shape is narrower than that from parallel connetion or single SiPM. Narrower pulse shapes imply a faster signal rise time, which is an important parameter in fast timing measurements [29]. Tests done with lasers, as well as literature studies [29], indicate that a serial connection of SiPMs should be used in order to improve the time resolution of the SciTil. If the SiPMs are connected in series, the signal output becomes faster and the pulse height drops because of the reduced total capacitance. There is always a compromise to be made, regarding the number of SiPMs connected in series. Adding more SiPMs in series causes the number of dark counts to increase and, at some point the signal rise time will stop improving. As shown in Fig. 5.7, the signal rise time does not improve significantly between 3 and 4 SiPMs in series, therefore it was decided to only use 4 SiPMs, as adding more in series would not have made an improvement.

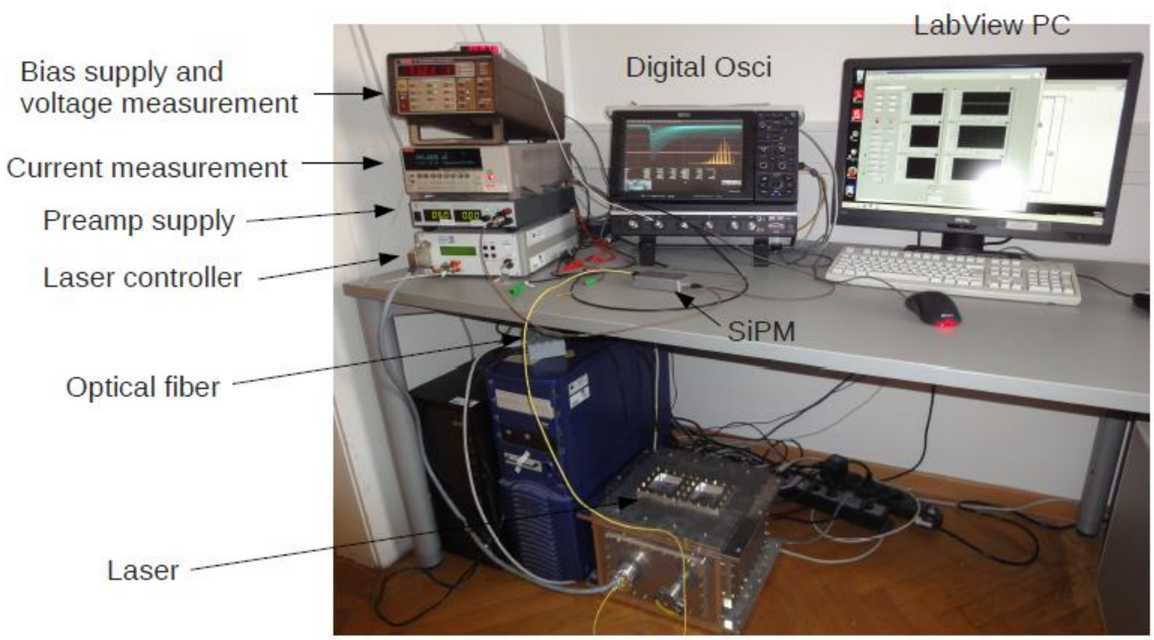

Figure 5.10: Measurement setup for testing SiPMs signal rise time in different connection configuration. The laser light (λ=404 nm) was guided through an optical fiber to a small light-tight metal box to illuminate the SiPMs. Figure adapted from [31].

5.3. Voltage amplifier

A voltage amplifier specially designed for fast timing applications has been adapted and built in order to amplify the signal coming from the SiPMs. An efficient preamplifier does not deteriorate the signal rise time and keeps the noise as low as possible. An important electronic property of the SiPM is that for a 3x3 mm^2 sensor the output capacitance is above 300 pF, which is much larger than the typical PMT 10 pF output capacitance. Also when incident light triggers the SiPM pixels, some of the APDs are fired while others remain inactive. Depending of the fired/unfired number of APDs, the total output impedance of the SiPM varies with the amount of light hitting the sensor. As a result of this, the amplifiers should be designed to have less input impedance in order to have a faster and a better linearity of the signal. The following amplifier was optimized for fast timing application and three different versions were custom made: one was built in the UK by a private company, one in Vienna by the electronics specialist Herbert Schneider and one by the Institute in Erlangen (see Fig. 5.12) [32].

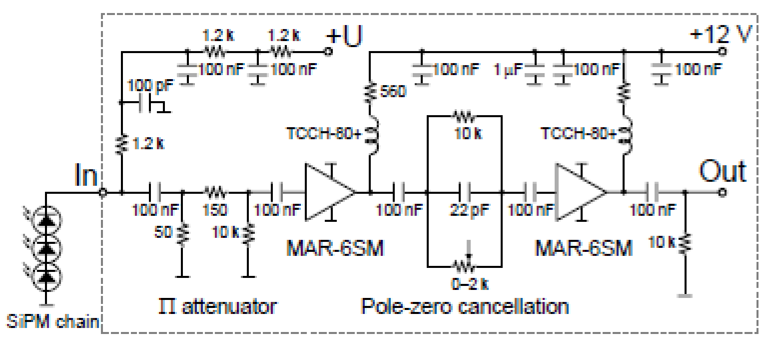

Figure 5.11: PSI amplifier circuit diagram adapted from [29].

The signal input is amplified two times by the MAR-6SM wideband amplifiers and is transmitted to the output signal. The preamplifier board provides also bias for the SiPMs through the signal line. The preamplifier itself needs 12 V in order to be operational [29]. The pulse shape of the signal was optimized with the pole-zero cancellation method. For optimizing the pulse shape one needs to connected the output signal to the oscilloscope and analyse the signal rise/fall time.

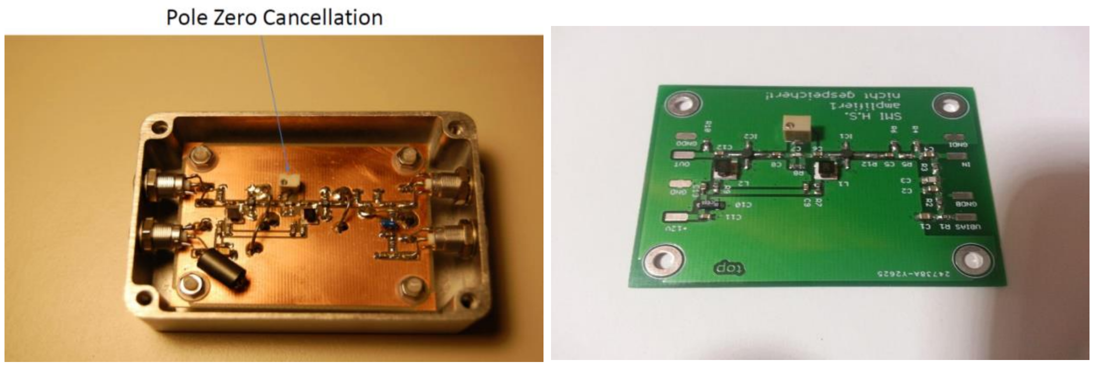

Figure 5.12: Picture with the reproduced PSI amplifier board. The pole zero cancellation shaping the signal with its variable resistence. Amplifier built by H.Schneider (left) and amplifier built by a company from England

The PZC has a variable resistance and can be operated between 0-3000 Ohm.

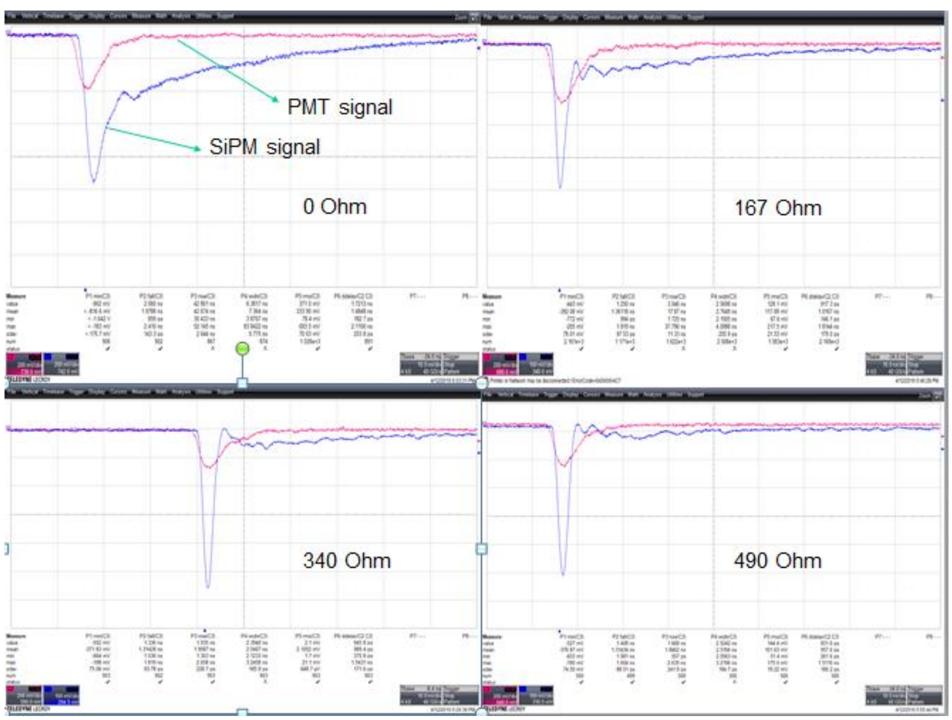

Figure 5.13: Picture taken from oscilloscope. Pulse shape optimisation of the SiPM signal for fast timing application. By increasing the resistance of the PZC up to 490 Ohm, the signal rise and fall time improves and the baseline is stabilized faster (impedance matching). The output signal is coming from board containing 4 SiPMs in serial configuration with S13360-3050PE SiPMs.

In Fig. 5.13, the screenshots taken by the oscilloscope indicate that if the resistance of the pole zero cancelation is increased, the efficiency of the amplifier improves and the signal baseline is rapidly stabilized.

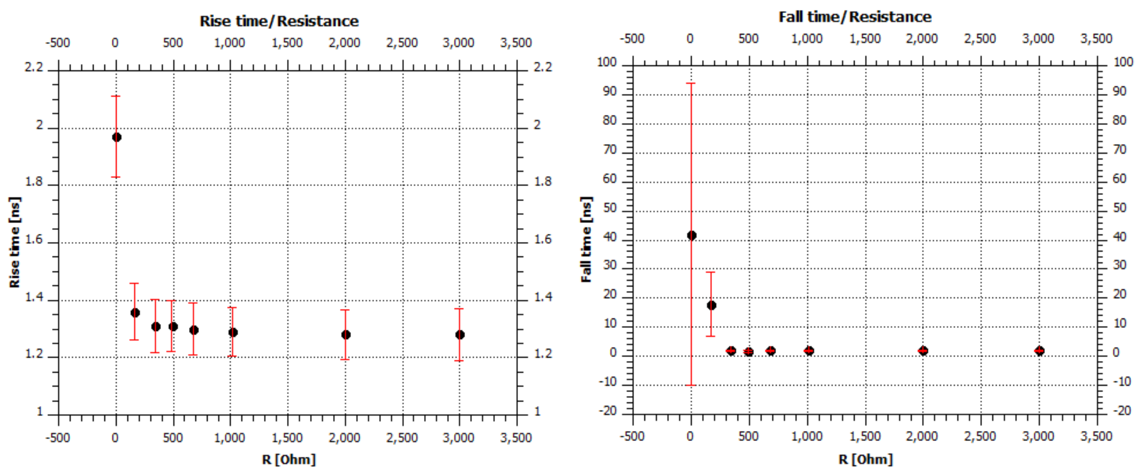

Figure 5.14: Signal rise(left) and fall (right) time in dependency of resistance value. The plots show, that an impedance matching is required in order to operate the amplifier at its maximum potential. A value of 500 Ohm was selected. **Optimized signal rise time 1.3 ns for PSI amplifier**.

The time resolution of the detector improves with decreasing signal rise time and therefore the measurement from Fig. 5.14 indicates that the optimal value is around 500 Ohm.

5.4. Time resolution studies with serial and hybrid configuration

Several experimental studies have been carried out in the laboratory in order to evaluate and understand the limiting factors of the time resolution. The single tile prototype is constituted of 1 scintillator readout by 4 SiPMs on each side. In order to evaluate the time resolution, various prototype configurations were tested: different scintillator material (EJ-228, EJ232, $30x90x5\ mm^3$), SiPM connection (serial, hybrid), voltage amplifiers (PHOTONIQUE, PSI) and different SiPMs.

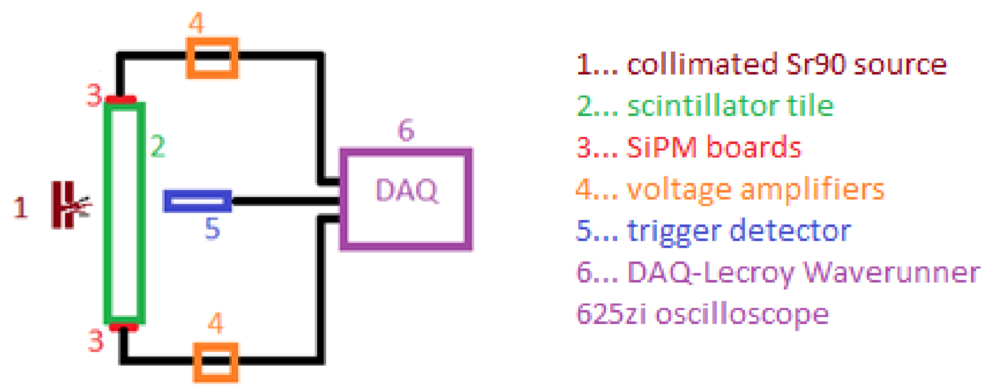

Figure 5.15: Schematic view of the experimental setup. Highly collimated beam of electrons penetrate through the center of the scintillator. The resulting light is collected by the sensors attached to left and right side of the scintillator.

A $^{90}\mathrm{Sr}$ source was used to provide a highly collimated (1 mm cavity) beam of electrons. The hit position of the electrons was the center of the scintillator. The generated light in the scintillator was captured by 4 SiPMs (S13360-3025PE and S13360-3050PE, respectively) on each side. The output signal was amplified and transmitted to the oscilloscope. The registered waveforms by the oscilloscope were saved as ASCII files and fitted in root [33]. The Trigger signal for the prototype was a HAMAMATSU PMT (H3167BX, bias voltage: 1500V) with a small scintillator (BC-408, 3x3x5 mm^3) attached to it. The time resolution of the single scintillator tile prototype is calculated as indicated in eq 3.5. An ISEG ECH238 power supply was used to bias the PMT and SiPM boards. The purpose of this measurement was to see if there is any difference in time resolution when using the hybrid or serial connection and to test the signal rise time with PSI and photonique amplifiers.

The experimental setup is shown in Fig. 5.15. Firstly, the hybrid configuration with four Hamamatsu SiPMs (S13360-3025PE) was tested. For this measurement the PSI-amplifiers were used. Internal noise as well as external noise is always an issue when dealing with fast timing measurements. In the following screenshot (Fig. 5.16) taken with the oscilloscope, the signal noise can be visualized.

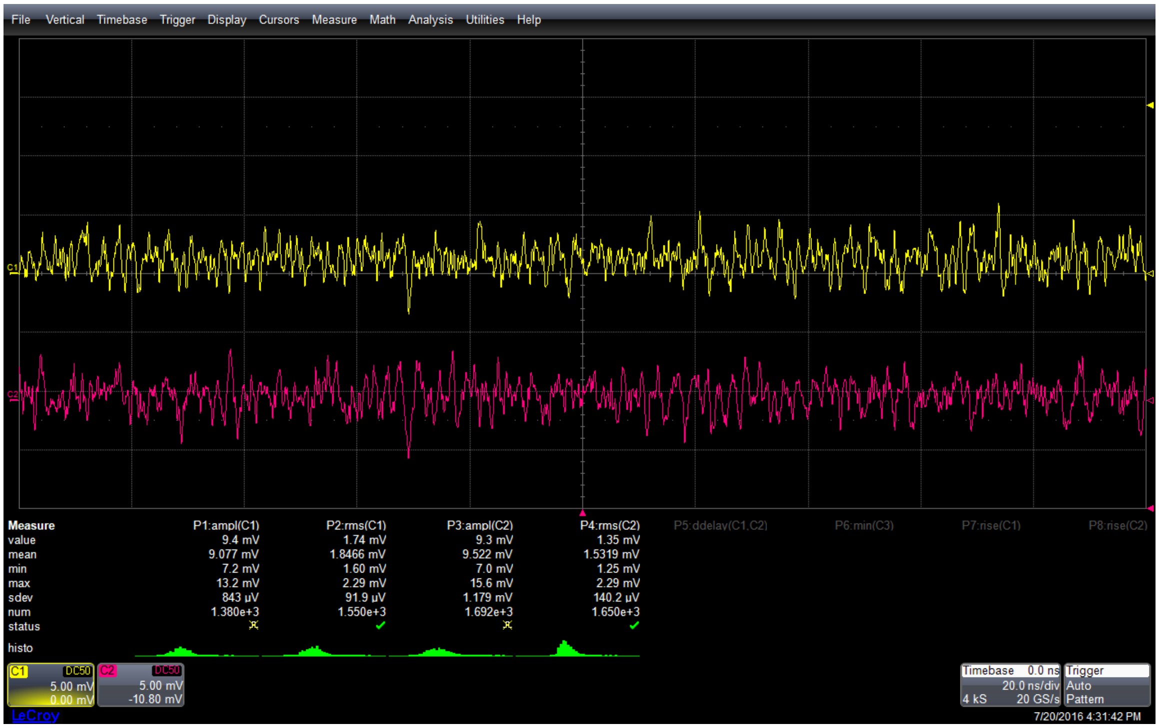

Figure 5.16: Screenshot from oscilloscope measuring the signal noise level of the PSI amplifier. Yellow (C1) is the noise coming from the left board after amplification and the pink one is coming from the right board. The SiPMs were not biased.

The noise can be evaluated in two ways (see Fig. 5.16). One can look at its amplitude by measuring the peak to peak level, or just take the rms (root mean square) of the whole data, which is a more consistent method. The peak to peak noise of the signal was about 10 mV/Channel and its rms 1.8 mV/Channel. For sensitive fast timinig measurements this is a relatively noisy environment, which could degrade the time resolution.

A pattern function between the three Channels (signals coming from the two channels of the scintillator prototype and PMT) was used to trigger the data acquisition. The threshold level was set to -40 mV. In the following oscilloscope screenshots the pulse shape of the SiPMs can be visualized:

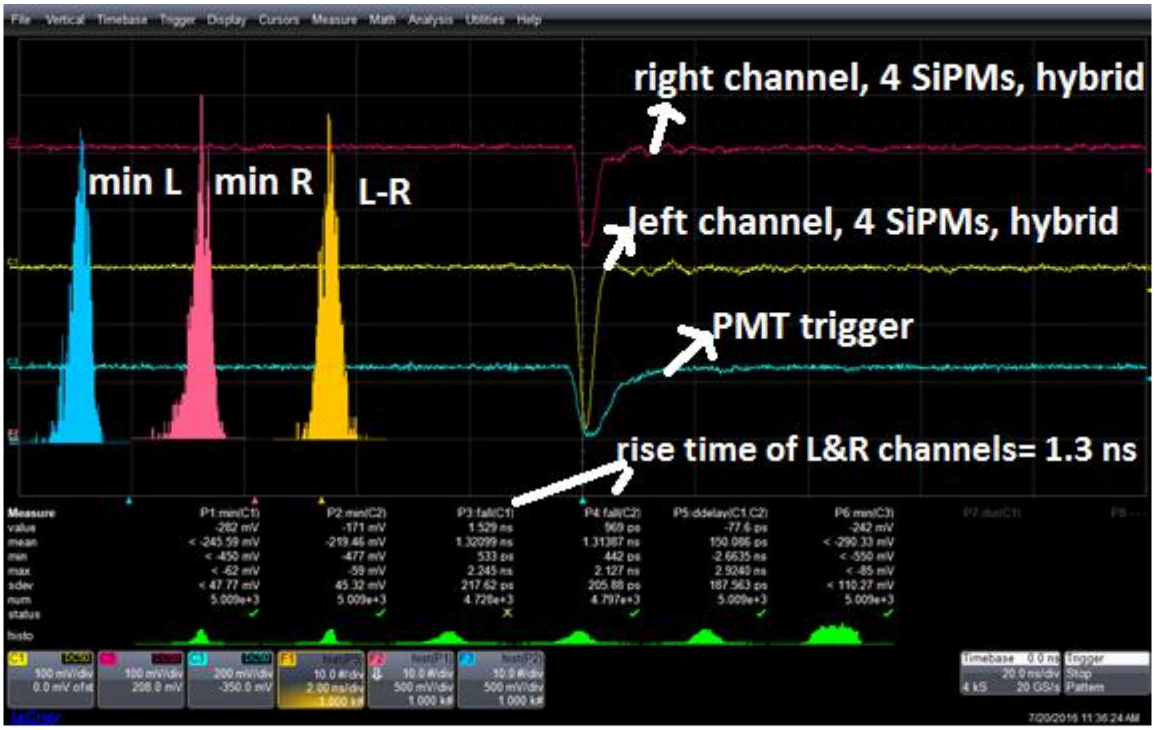

Figure 5.17: Pulse shapes of right sensor board (pink signal), left sensor board (yellow) and trigger detector (C3, blue). The yellow histogram (L-R) shows the time difference between left and right channel. The pink and blue histograms give information about the pulseheight of the two channels. The signal rise time is about 1.3 ns with PSI amplifiers.

The goal of this measurement is to calculate the time resolution of the scintillator counter. For this, the oscilloscope used a delta delay function, which measures the delay between the two signal amplitudes (yellow and pink, see Fig. 5.17). The resulting histogram (yellow histogram, see Fig. 5.17) was then fitted with a gausian function to extract the standard deviation, which is the time difference resolution. Half of this value will give the detector time resolution (see eq. 3.5). To get information about the detector light yield, the pulse height of the signals must be measured. For this, the oscilloscope used a minimum function (see Fig. 5.17, blue and pink histograms). In order to see the correlation between pulse height and number of detected photons, a single photon measurement is required. Unfortunately, the single photons were not visible because of the high noise. The measurement includes a bias voltage scan and a pulse height profile. An optimum applied bias voltage on SiPMs is of particular importance when optimizing timing measurements. The serial and hybrid connection was tested.

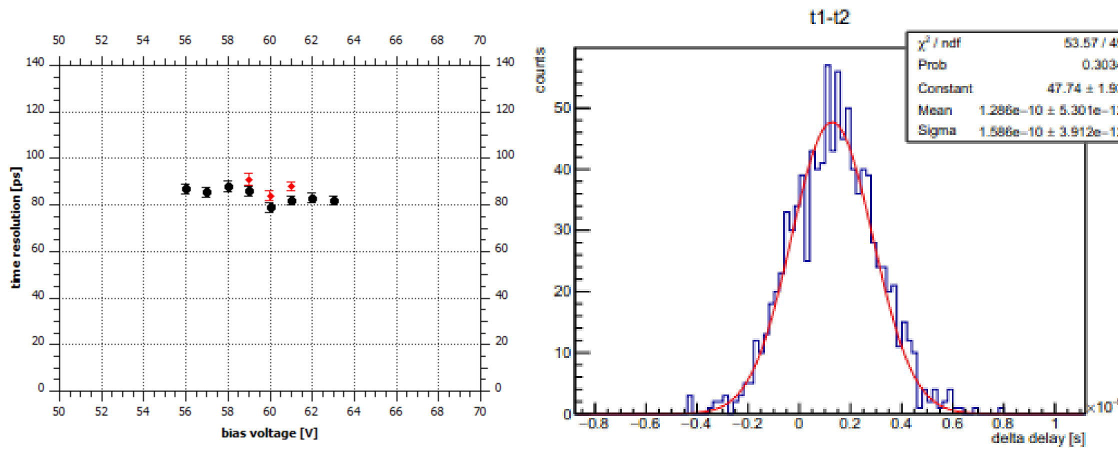

Figure 5.18: Time resolution dependency on applied bias voltage to the SiPMs. Red points represent the time performance obtained with EJ-228 scintillator and black points with EJ-232 (left picture). The time difference resolution 158 ps (L-R, 5000 events) at optimum bias voltage 60 V (right figure). The time resolution (best value) of the scintillator counter can be estimated at 79 ps (EJ-232). Hydrid connection board with S13360-3025PE SiPMs, PSI amplifiers.

Also in a similar fashion, the signal rise time, pulse height and time resolution was calculated also for the serial connection board.

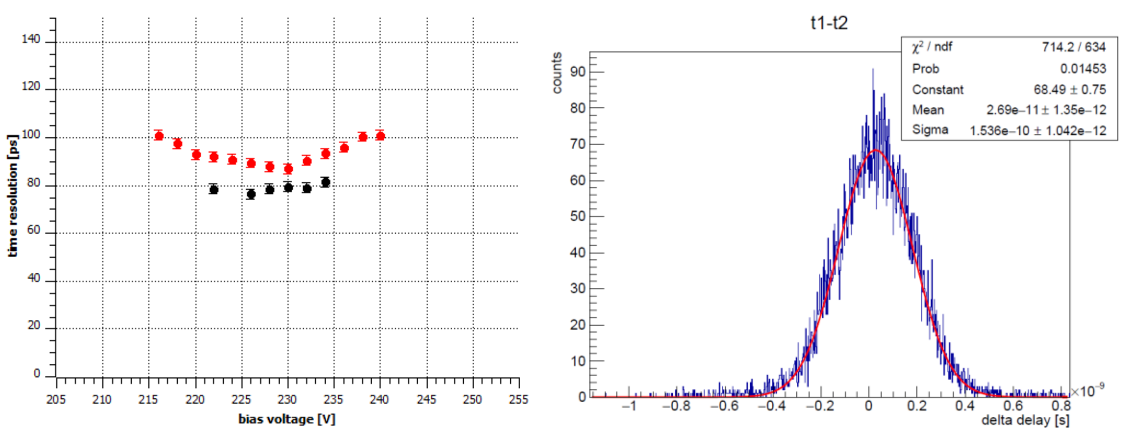

Figure 5.19: Time resolution dependency on applied bias voltage to the SiPMs (left picture). Red points represent the time performance obtained with the EJ-228 scintillator and the black points with the EJ-232. Time difference resolution 154 ps (left channel minus right channel, 5000 events) at optimum bias voltage (226 V). The time resolution (best value) of the whole detector can be estimated at $\frac{154}{2} = 77$ ps (right figure). Serial connection board with S13360-3050PE SiPMs, photonique amplifiers.

The measurement indicates that there is no significant difference in time resolution between the two different connection configurations. Both serial and hybrid connections achieved time resolutions of ∼ 80 ps.

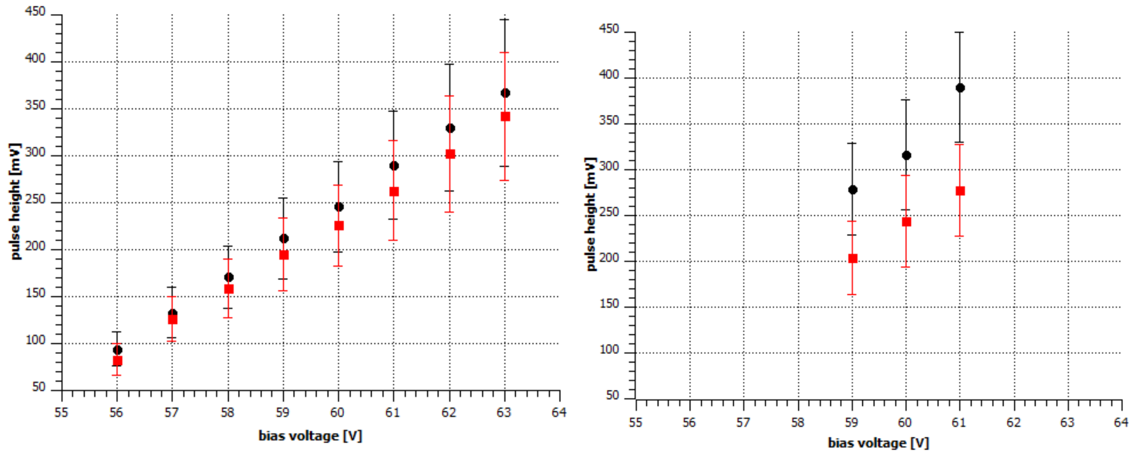

Figure 5.20: Pulse height spectrum. Signals coming from Ch1 (red values) and Ch2 (black values) are shown. Left picture represents values obtained with EJ-232 and the right one with EJ-228 scintillator. Hydrid connection board with S13360-3025PE SiPMs, PSI amplifiers.

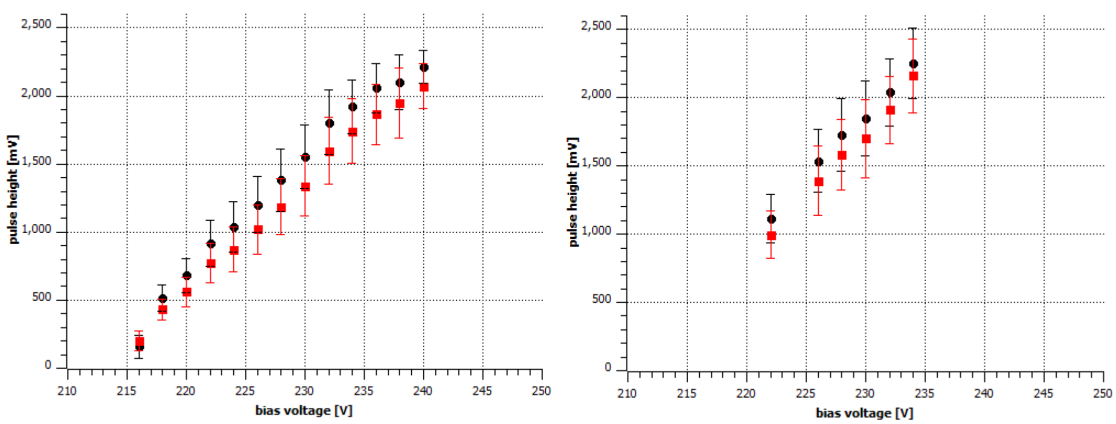

Figure 5.21: Pulse height spectrum. Signals coming from Ch1 (red values) and Ch2 (black values) are shown. Left picture represents values obtained with EJ-232 and the right one with EJ-228 scintillator (replce over voltage with real voltage applied). Serial connection board with S13360-3050PE SiPMs, photonique amplifiers.

For the serial connection the voltage amplifier used was the photonique preamplifier. An advantage of this preamplifier was that the noise level was lower (3 mV peak to peak level, 600 μV rms) than with the PSI amplifier (10 mV, 1.8 mV rms), but the signal rise time was worse (3 ns). A summary of the measurement can be seen in Table 5.1. In comparison with EJ-228, EJ-232 had a better time resolution but the light yield was worse because of stronger light attenuation (see scintillator properties in Table 3.1). When using the S13360-3025PE SiPMs the resulting pulse height dropped significantly (see Fig. 5.20) mainly because these SiPMs have lower gain (see table 4.1 with SiPM properties).

Connection type	Preamplifier type	SiPM Type	Bias voltage[V]	Rise time [ns]	Noise level, peak to peak [mV]	Best time resolution [ps]
Simple serial	PHOTONIQUE	S13360-3050PE	$\sim$240	3 ± 0.3	$\sim$3	77 ± 2
Hybrid connection	PSI	S13360-3025PE	$\sim$60	1.2 ± 0.2	$\sim$10	79 ± 2

Table 5.1: Comparison between serial and hybrid connection of the SiPMs

This was a way of testing the time resolution of the scintillator prototype by using the oscilloscope. The differences between a commercial oscilloscope and a waveform digitizer when the pulse shape is being evaluated is as follows: "The digitizers allow for dead-timeless acquisition. In the digitizers, all the channels are allowed to generate triggers independently. The digitizers are designed for scalability. They have high bandwidth data readout links and on line data processing"[6]. Nevertheless results indicate that a good time performance is possible. It was clear that with an optimal experimental setup one could achieve even better results. The limiting factor may be the high noise, which can be avoided if the experiment is carried out in a laboratory with optimal features. Since the signal rise time plays an important role in time resolution, the PSI amplifier has been chosen for the next measurements. The signal rise time values shown in table 5.1 depend soley on the amplifiers and not on connection type (simple serial vs. hybrid). A complete measurement will be presented next in chapter 6, where the position depending time resolution as well as number of detected photons is calculated.

[6] http://www.caen.it/servlet/checkCaenDocumentFile?Id=9532; 2014

Chapter 6

6. Measurement at Erlangen, single tile optimization

6.1. Experimental setup

It should be noted, that the measurement was done in collaboration with the Erlangen Center for Astroparticle Physics (ECAP). The results are being included in the TDR of the barrel TOF detector [15]. Our colleagues from Erlangen Institute have a remotely controlled stepper motor, which could move the source of electrons in x,y direction and therefore the time resolution could be measured across the whole scintillator surface. The goal of this measurement was to optimize the time resolution of the single tile prototype. In order to evaluate the performance of the single tile, various parameters had to be adjusted: scintillator material, SiPM bias voltage, reflector material for scintillators, electronics threshold and the position dependent time resolution. The laboratory in Erlangen is located in the basement of the physics institute in the hall of an old Tandem accelerator that was shut down in 2015 and it is well suited for measurements due to its constant temperature, lack of wifi and restriction on mobile phone usage. The prototype measurements were taken in a big dark box shielded with copper in order to avoid any external noise (see Fig. 6.1)

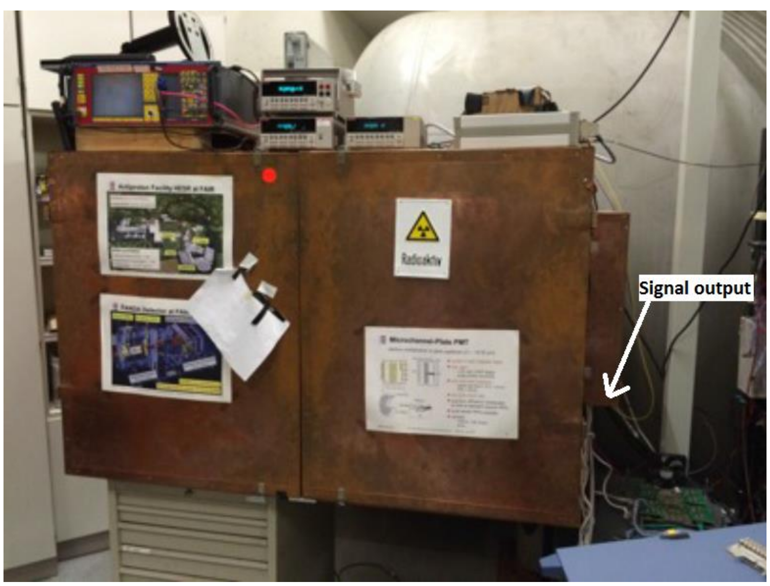

Figure 6.1: The measurement setup inside the shielded box in order to avoid external noise.

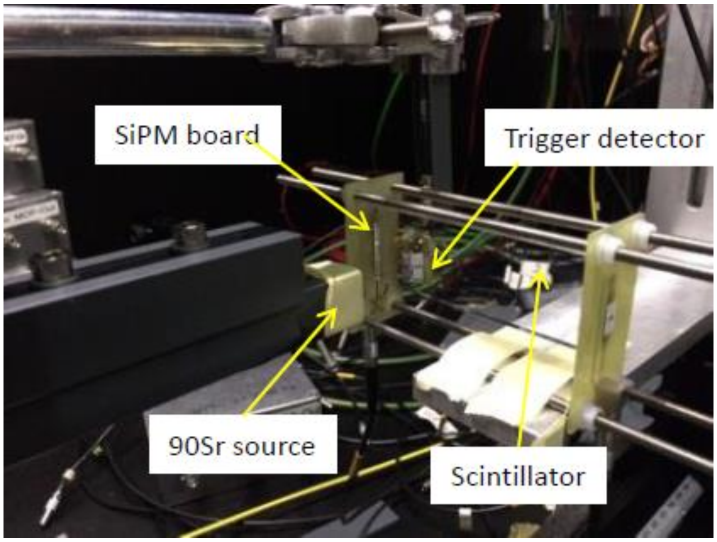

Figure 6.2: Experimental setup. With a variable platform (in x,y direction) under PC control, the source coupled with the trigger detector can be moved in order to adjust different hit positions on the scintillator. The scintillator tile was fixed.

A layout of the experimental setup is being shown in the figure below.

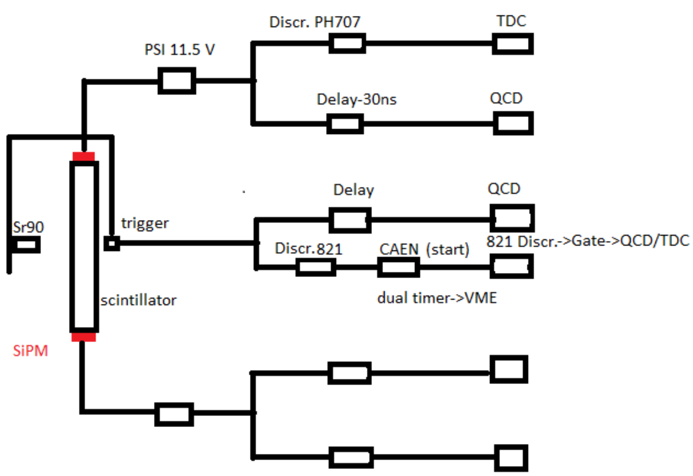

Figure 6.3: Experimental setup scheme containing source, trigger, SciTil prototype and read-out electronics

A highly collimated ^{90}Sr source (1mm window) is used to provide a beam of electrons. The source is mounted with the trigger detector on a xy-stage to define the hit position of electrons on the scintillator. The trigger detector uses a small scintillator (5x5x5 mm^3) readout by a single SiPM (HPK S12572-050P). The scintillator tile (90x30x5 mm^3) is readout from both sides by SiPM boards, each of which contains four HPK SiPMs (S13360-3050PE) connected in series. The SiPMs are attached to the scintillator with optical grease (BC-630). With the experimental setup shown in Fig. 6.2, the time resolution across the whole scintillator surface can be measured. The beam of electrons produces low intensity light in the scintillator. This light is captured by the SiPM chains and transmitted to the amplifiers (see Fig. 6.3). After the amplification, the signal is split in two channels (see Fig.). One channel is connected to a QDC (CAEN V792). The second channel is connected to a leading-edge discriminator (Philips Scientific 707), which can provide threshold control for negative signals between -10 mV and -1 V to provide the start signal for the TDC (CAEN V775). In electronic instrumentation and signal processing modules like the TDC (which measures the leading edge of fast signal and gives the time stamp) and QDC (the integrated signal is proportional to the charge, which is related to the number of photons detected by the sensors) are indispensable. The front end electronics consists of a Crate, VME modules, discriminators, a power supply and an oscilloscope and can be seen in Fig. 6.4:

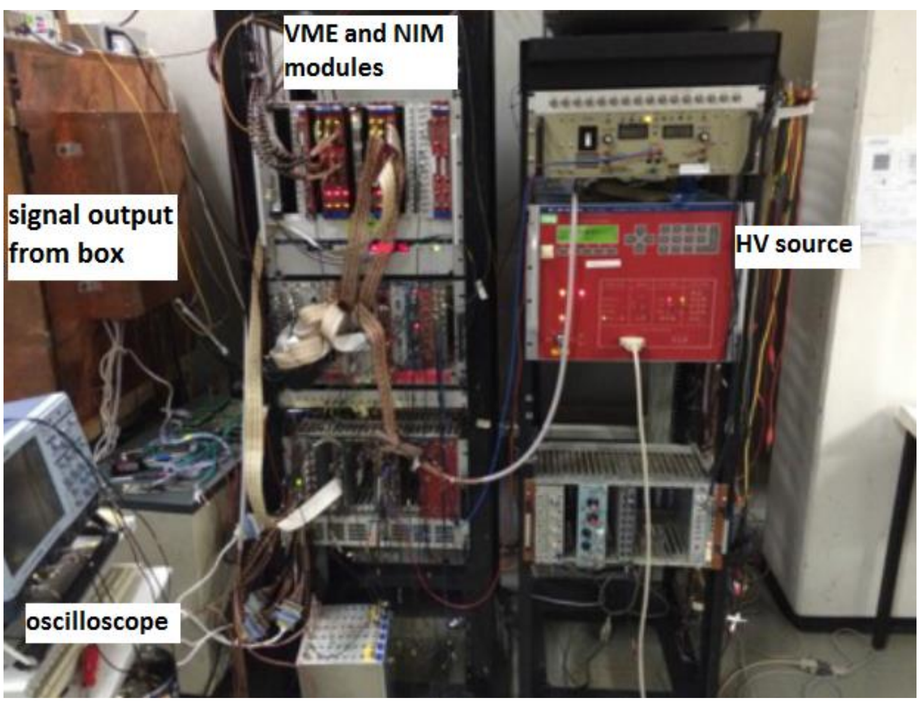

Figure 6.4: Front end electronics: HV source, VME and NIM modules, digital oscilloscope.

The time resolution of the single tile prototype is calculated by using the formula (3.5) shown in the previous chapter. A picture with the amplified signal has been taken from the oscilloscope in Fig 6.5.

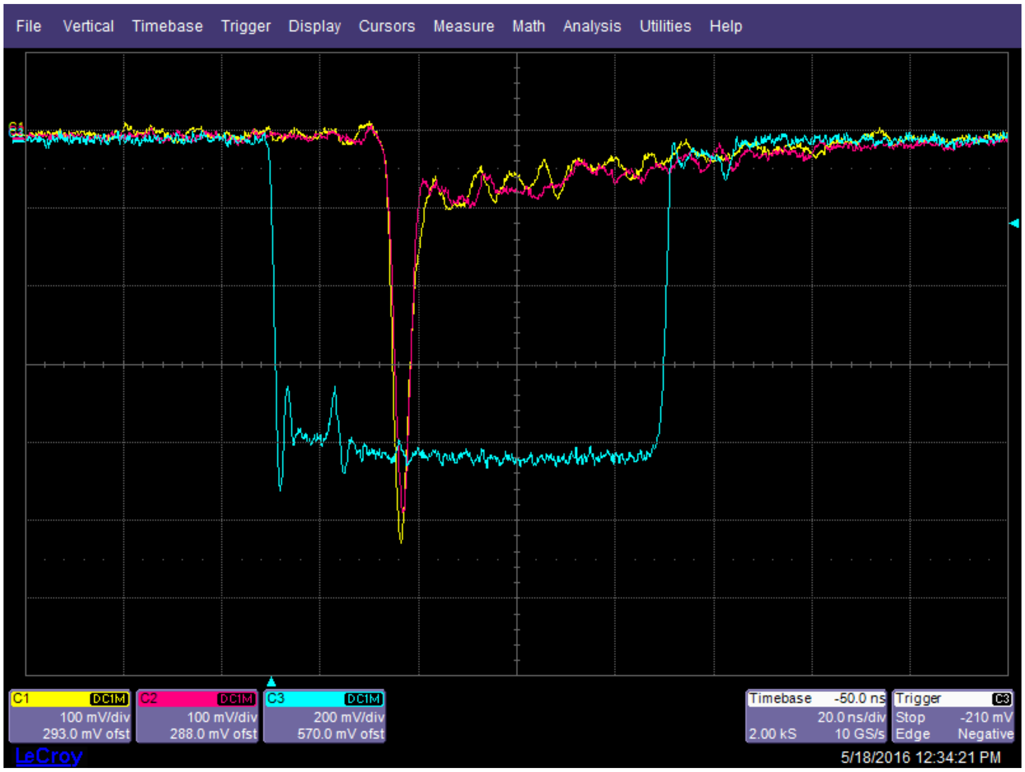

Figure 6.5: Trigger signal (blue) and analog signal from the two sensor boards (yellow and pink)

In Fig. 6.5 three signals are being shown. The blue digital signal is from the trigger detector. It provides the start signal for the TDC and also controls the width of the QCD gate. The width of the QCD gate should include the whole signal, until the baseline is stabilized again (about 100 ns in this case). The yellow and pink pulse shapes are the analog signals from the sensor boards after the amplification.

6.2. Single photon spectrum

In order to see the correlation between the pulse height [QDC channels] and number of detected photons, a single photon spectrum is required. For this purpose, the beam of electrons was replaced by a pulsed laser, whose intensity could be lowered until only single photons were visible. By measuring the distance between peaks (see Fig. 6.6) the correlation between QDC channels and single photo-electrons can be determined. With 20 times amplification, a single photon-electron corresponds to 2.3 QDC channels or 0.22 pC for Channel 1 (left sensor board). For Channel 2 (right sensor board) a photo electron corresponds to 2.5 QDC channels or 0.24 pC.

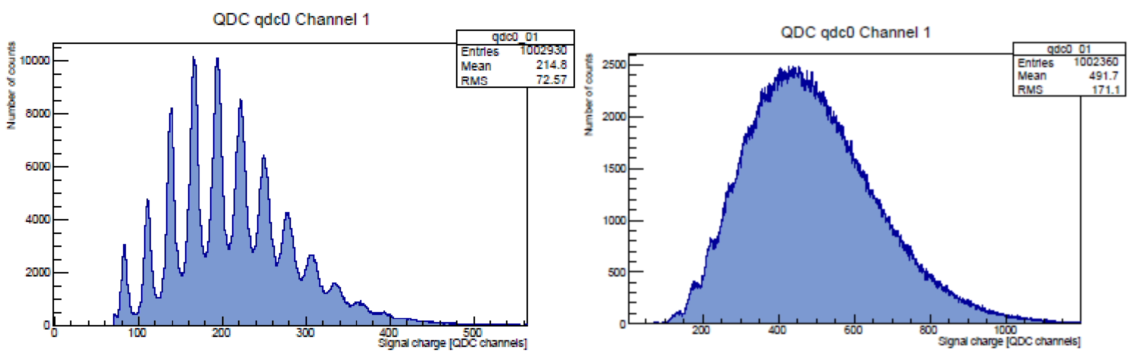

Figure 6.6: Single photon spectrum with 30 ns (left) and 100 ns (right) gate width of the QDC

In the right picture in Fig. 6.6 it is hard to differentiate between photo-peaks because the gate width of the QCD is to long (100 ns) and the noise level of the signal to high. Nevertheless, a rough estimation was still possible.

6.3. Electronic threshold, bias voltage scan and wrapping

The laser is now replaced by the electron source. Firstly, one should find the optimum bias voltage for the SiPMs and the electronics threshold. Two different scin-tillators (EJ-232 and EJ-228) specifically designed for fast timing measurements were tested. The two PCB boards, each with 4 SiPMs connected in series (S13360-3050PE) were attached to the scintillator. Dark counts are always an issue and therefore a very low threshold could deteriorate the time resolution and should be avoided. According to the following measurements a threshold between -30 and -50 mV and a bias voltage ranging from 230 to 250 V should be applied (see Fig. 6.7, 6.8). Nevertheless a full bias voltage scan is required in order to find the best time resolution.

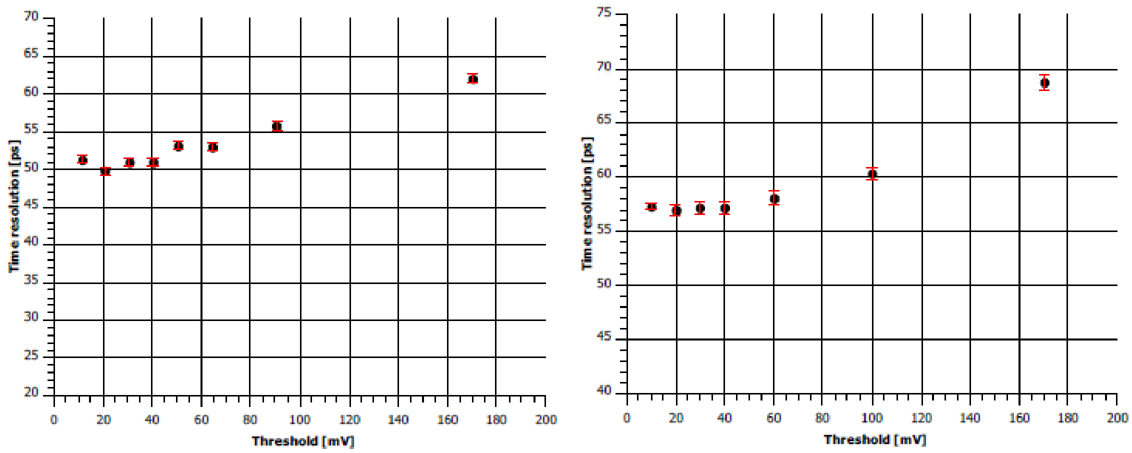

Figure 6.7: Time resolusion dependency on electronics threshold. The left picture shows results achieved with EJ-232 scintiilator at a bias voltage of 230V. The right picture illustrates the measurement taken with the EJ-228 scintillator at a bias voltage of 240 V.

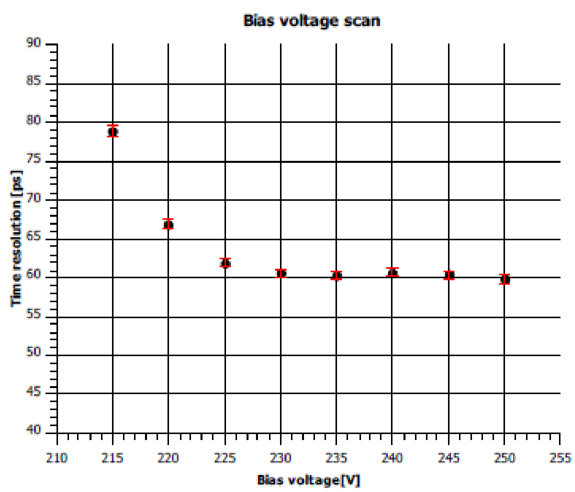

Figure 6.8: Time resolution depending on SiPMs bias voltage, EJ-228 scintillator.

The threshold scan shown in Fig. 6.7 already indicates that the scintillator EJ-232 provides a slightly better time resolution. The following measurement compares the time resolution and light yield obtained with both scintillators across 9 different points (2500 events recorded on each point).

First, the measurement was done with EJ-228- followed by EJ-232 scintillator.

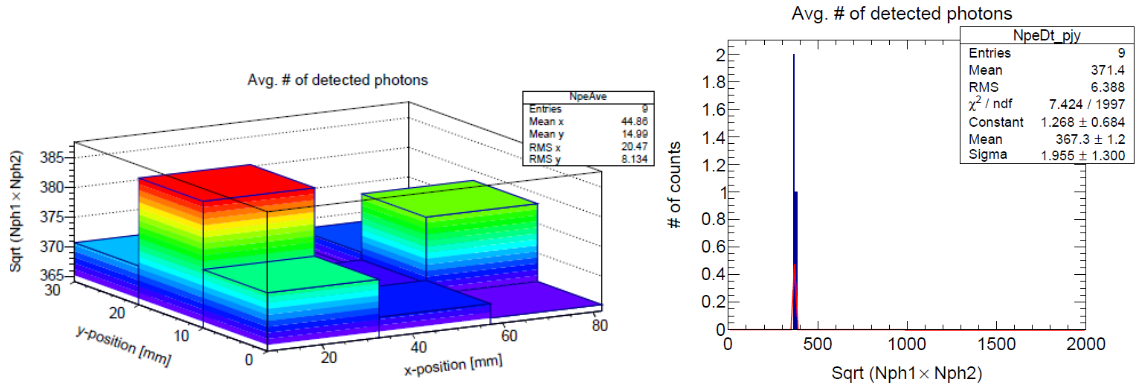

Figure 6.9: Average # of detected photons and the mean value from 9 positions (right), EJ-228.

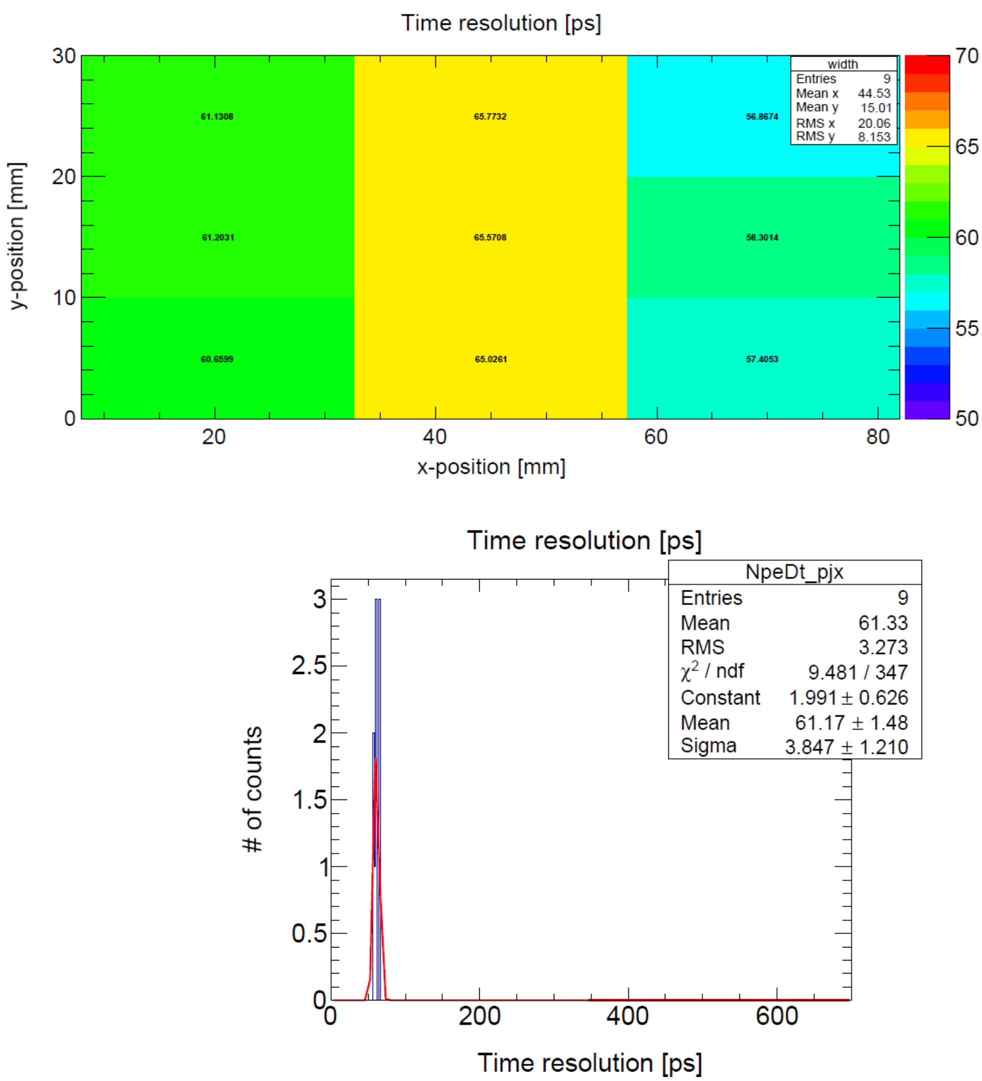

Figure 6.10: Mean time resolution of the 9 points distributed across the scintillator surface (top picture) and the histogram showing the mean value of this time resolutions (bottom), EJ-228.

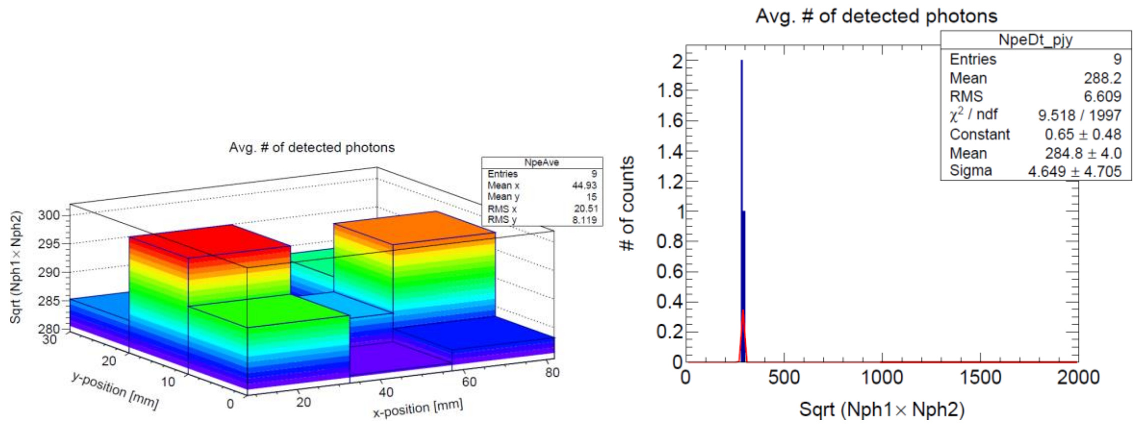

Figure 6.11: Average # of detected photons and mean value from 9 position (right), EJ-232.

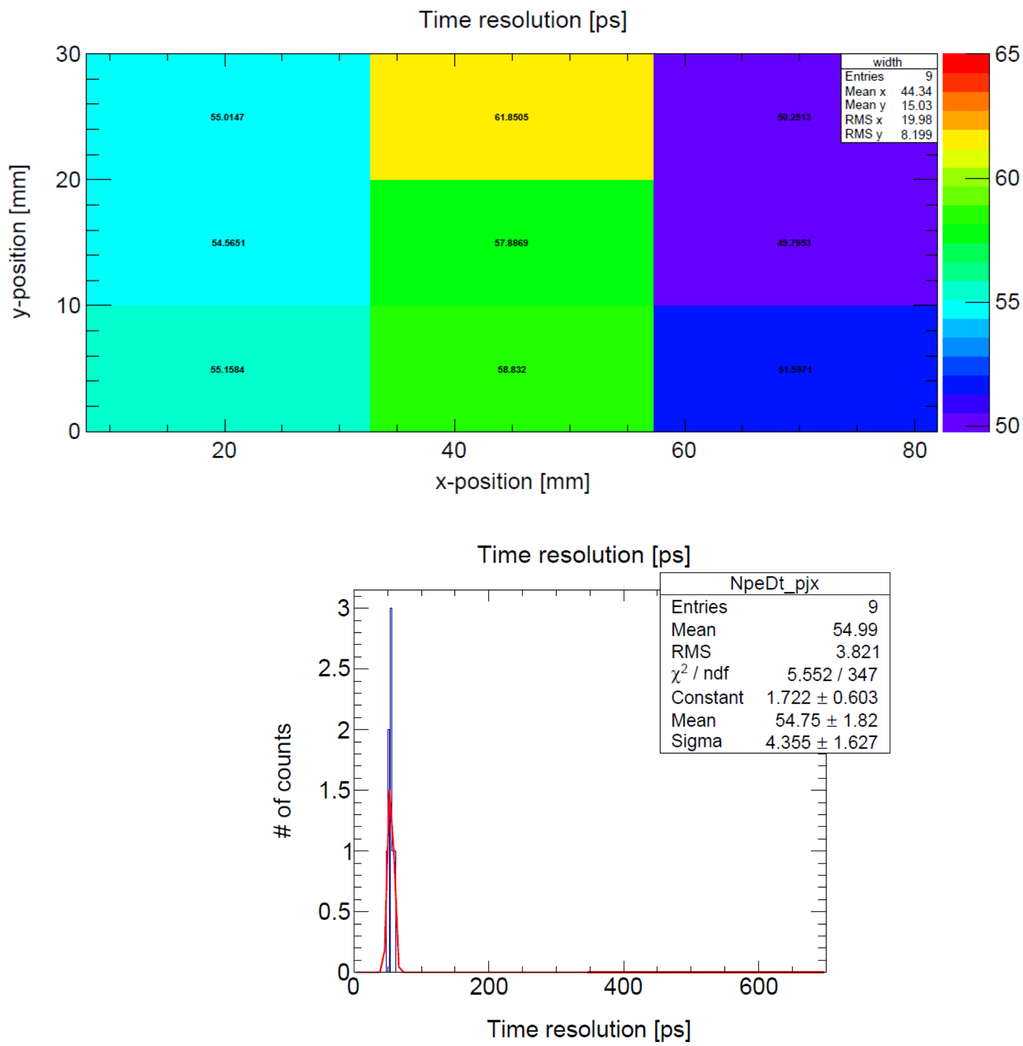

Figure 6.12: Mean time resolution of the 9 points distributed across the scintillator surface (top picture) and the histogram showing the mean value of this time resolutions (bottom), EJ-232.

A mean value of 367.3 ± 1.2 detected photons (see Fig. 6.9) and a mean time resolution of ~ 61 ps (see Fig. 6.10) was achieved with the EJ-228. With the EJ-232 scintillator a mean value of 284.8 ± 4 detected photons (see Fig. 6.11) and a mean time resolution of ~ 55 ps (see Fig. 6.12) was achieved. One can clearly see that the EJ-228 scintillator has a higher light yield, but a worse time resolution than the EJ-232. The rise time of the EJ-232 is shorter, which explains the slightly better timing performance.

The scintillators in their final design should be wrapped in reflecting material for protection purposes and for keeping the scintillators light tight. A variety of reflector combinations were tested on the two scintillators (EJ-232, EJ-228) and parameters, e.g. light yield and time resolution, were measured.

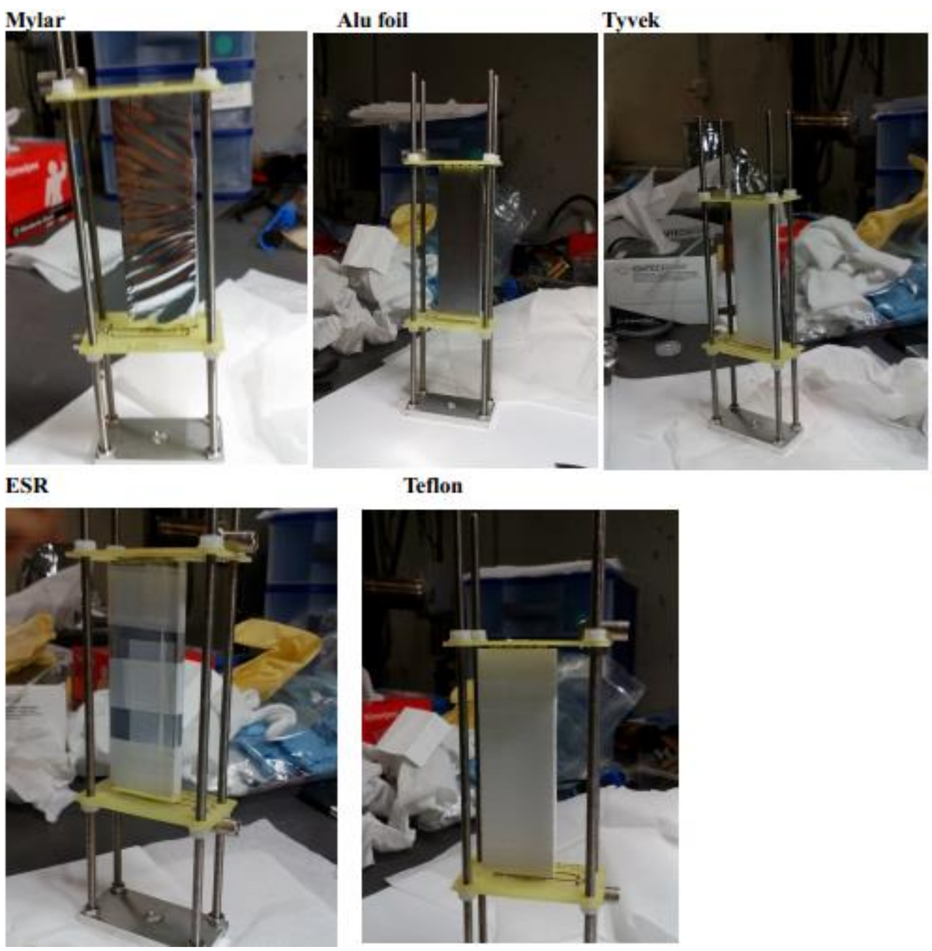

Figure 6.13: Single tile prototype with two sensor-boards and scintillator wrapped in different reflector materials.

The following reflector materials were tested: kitchen aluminum foil, aluminized mylar, Teflon tape, Tyvek hard structure 1057D, 54 g/m2, and Enhansed Speculiar Reflector (ESR). The results of the measurements are listed in Table 6.1 and represent the mean value from 9 different positions distributed across the scintillator surface. For teflon tape, three layers of the material were used, for the rest only one layer was applied.

Reflector type	Time resolution [ps]	Pulse height [QDC Channels]	Pulse height [# of detected photons]
No wrapping	55.0 ± 0.3	690 ± 12	288 ± 3
Aluminum foil	54.2 ± 0.3	821 ± 6	344 ± 3
Mylar	52.7 ± 0.3	848 ± 11	355 ± 3
Teflon tape	59.4 ± 0.3	975 ± 10	408 ± 3
Tyvek 1057D	55.0 ± 0.3	941 ± 8	394 ± 3
ESR	55.2 ± 0.3	847 ± 7	355 ± 3

Reflector type	Time resolution [ps]	Pulseheight [QDC Channels]	Pulseheight [# of detected photons]
No wrapping	61.3 ± 0.3	887 ± 10	371 ± 3
Mylar	59.7 ± 0.3	1063 ± 7	445 ± 3

Table 6.1: Time resolution and pulse height (EJ-232 top, EJ-228 bottom) of the single tile prototype using different reflector materials.

Aluminum foil, Teflon tape and Tyvek are commonly used for wrapping scintillators. ESR is a reflector material developed by the 3M company and is specially designed to ensure a light reflectivity of over 98% [35]. Despite ESR having such good properties, practically it was really hard to wrap the scintillators with it (material does not bend so easily) and at some points there were air gaps between scintillator and reflector material, which deteriorated its performance. With the scintillators wrapped in teflon tape, the highest number of photons was detected, but the time resolution did not improve. The aluminized mylar foil, with a reflectance of about 90%, delivered the best time resolution and for the rest of measurements this material was selected. The average number of detected photons of the single tile prototype is $N_{photons} = \sqrt{N_{ph\_l} \cdot N_{ph\_r}}$ with N_{ph_l} and N_{ph_r} representing the number photons of detected by the left and right sensor board, respectively. At this point all parameters (scintillator material, sensor quality and connection type, preamplifier, wrapping and electronics) were optimized.

6.4. Time resolution across whole scintillator surface

The following test was done with the optimum configuration: EJ-232 scintillator wrapped in aluminized mylar foil, WIEN amplifiers, a bias voltage of 240 V and electronics threshold of -30 mV. The stepper motor moved the beam of electrons across the whole scintillator surface (3069 positions) in 1 mm steps and registered 2500 events at each position.

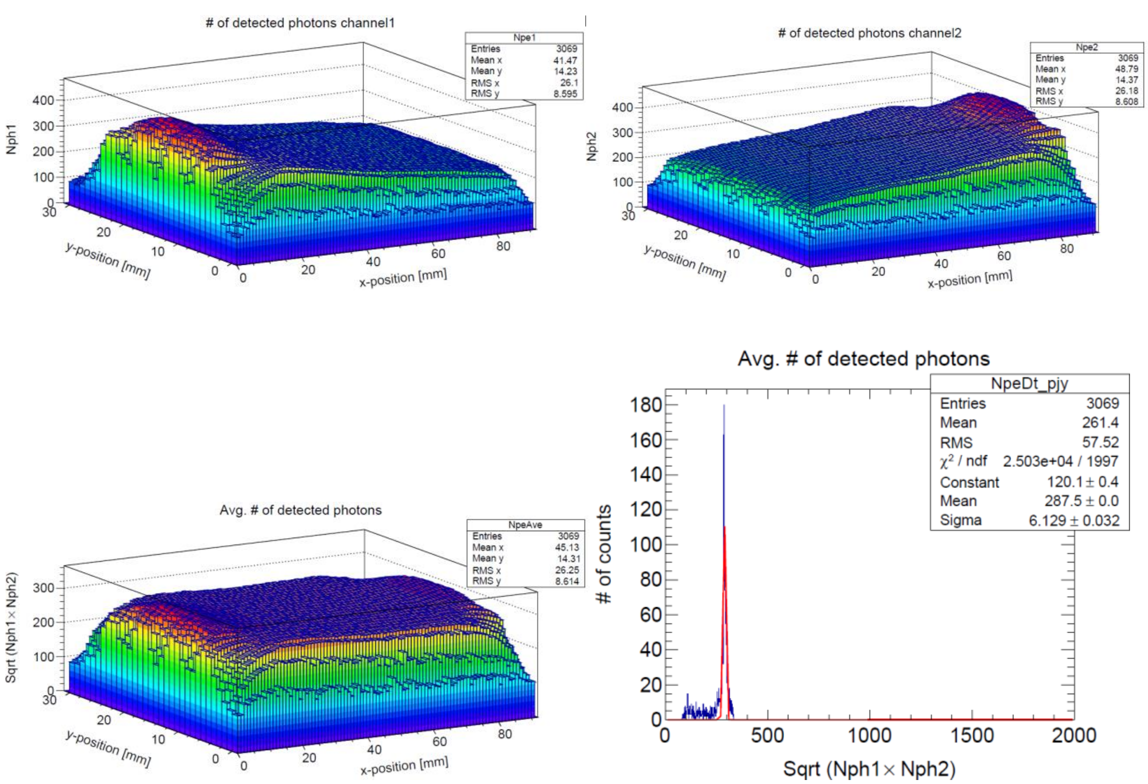

Figure 6.14: Number of detected photons on left and right channel (top); average number of detected photons (bottom), EJ-232.

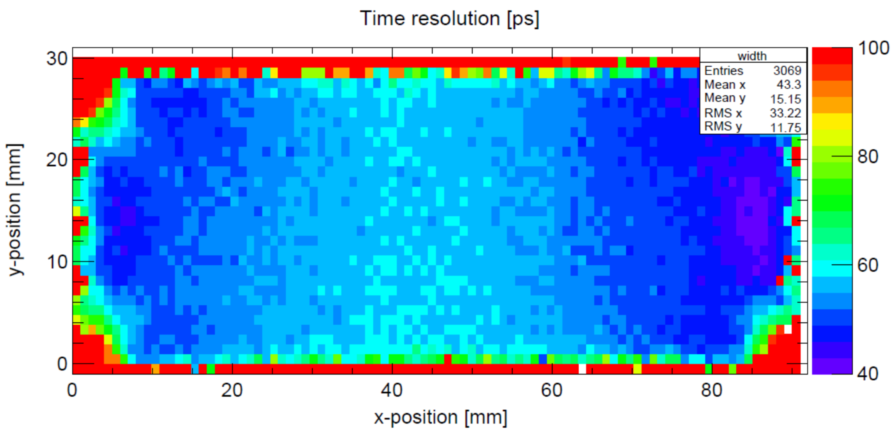

Figure 6.15: Time resolution distribution (3069 positions) across the whole scintillator surface(90x30 mm^2), EJ-232 scintillator tile readout by 4 HPK SiPMs attached on left and right scintillator side, EJ-232.

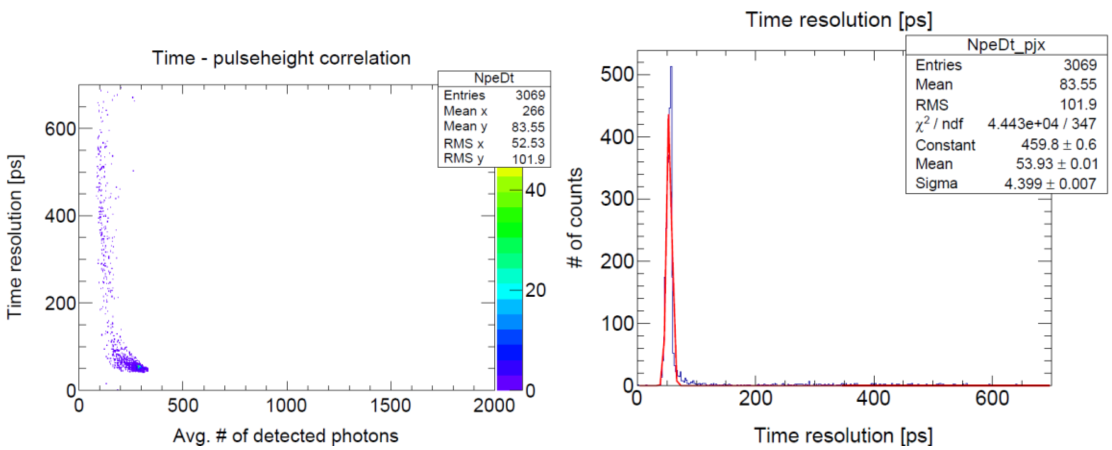

Figure 6.16: Correlation between time resolution and average number of detected photons (left), extracting the mean value from a histogram filled with 3069 time resolutions (right), EJ-232.

With this configuration a mean time resolution of $\sim$54 ps (see Fig. 6.16, 3069 time resolution values filling the histogram and fitted with a gausian function to extract the mean value) was achieved and detected 288 photons on average (see Fig. 6.14). From Fig. 6.15 one can tell that the time resolution was distributed almost homogeneously across the scintillator surface (values between 45-60 ps), depending on the hit position of the highly collimated electron beam. In the middle of the scintillator values of 60 ps can be seen. This is because the light is more likely to undergo more reflections until it reaches the SiPMs and this could cause a degradation of time resolution. An undesired effect was seen on the edges of the scintillator, where the time resolution exceeded 100 ps (see Fig. 6.15). This is due to the fact that electrons hitting the rims of the scintillator do not produce as much light in the scintillator as those hitting the centre. This effect leads to a decreasing pulse height and a worse time resolution. On the left, in Fig. 6.16, the correlation between pulse height and time resolution can be seen. The more detected light, the better the time resolution. Again due to some border effect of the scintillator, at some points the light yield and time resolution got worse. Nevertheless, including all raw data the results are quite satisfactory. The measurement was repeated also with the EJ-228 scintillator where a mean time resolution of 60 ps was achieved (see Fig. 6.17, right) with about 400 detected photons on average (see Fig. 6.17, left). The light yield is higher with the EJ-228 scintillator (less attenuation).

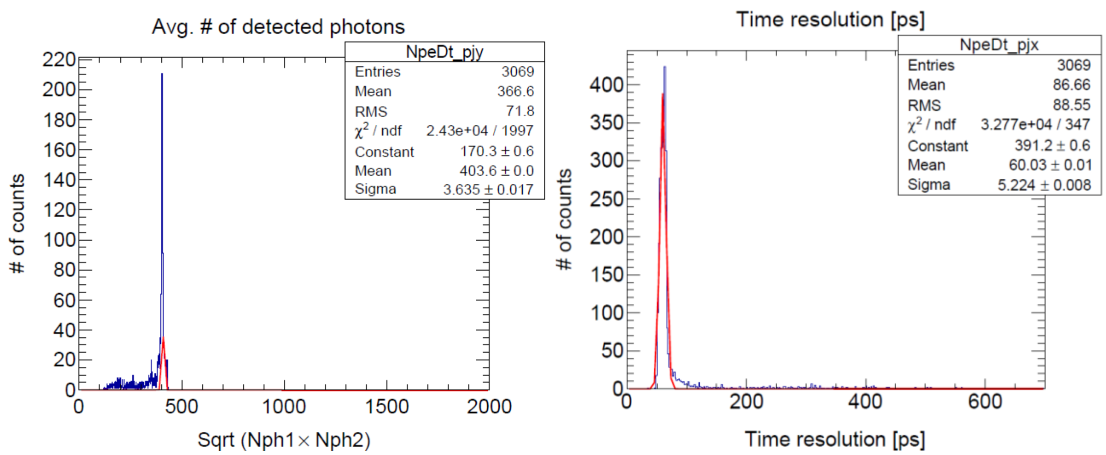

Figure 6.17: Average number of detected photons (left) and time resolution (right). Both histograms were fitted with a gausian function in order to extract the mean value of 3069 points, EJ-228.

A detailed and complete measurement has been done in order to optimize all necessary material and improve the performance of the detector.

Chapter 7

7. Beamtime test

Our institute regularly does experiments at the CERN east counter hall, area T10, in order to test detectors. In June 2016 we had the opportunity to do a first test with the new design of the SciTil under a beam of various particle species (p, $\bar{p}$, $K^{+/-}$, $\pi^{+/-}$, $\mu^{+/-}$, $e^{+/-}$ etc.) with a momentum of 6 GeV/c [13]. The goal of this measurement was to determine the time resolution of the SciTil under a beam of high energy particles, in order to have similar conditions as planned for the PANDA experiment. Because this beam time was dedicated to test detectors for the ALICE project, time for testing SciTil was limited. Nevertheless, a single measurement was done with the already optimized scintillator tile: EJ-232 scintillator (30x90x5) wrapped in aluminized mylar, sensor boards with 4 SiPMs in series (S13360) and PSI amplifier.

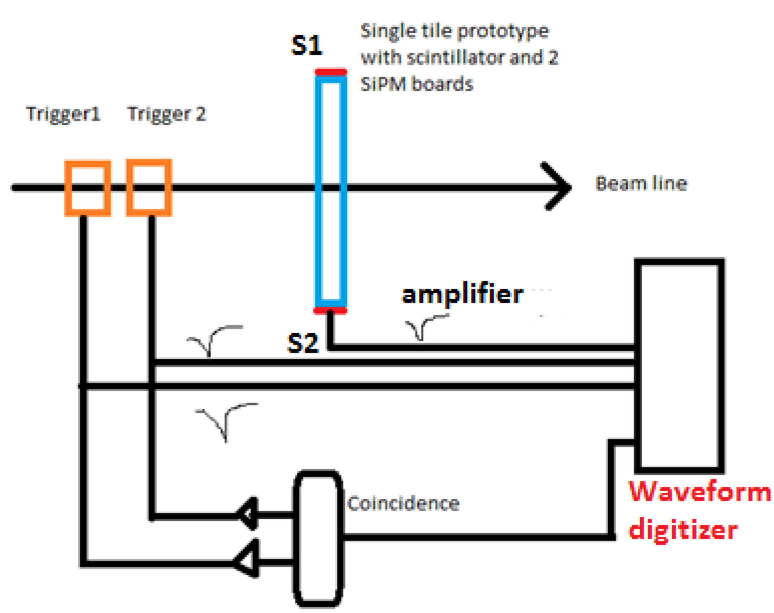

Figure 7.1: Experimental setup: trigger detectors with channels T_1 (trigger detector 1) and T_2(trigger detector 2), scintillator prototype with channels $S_1$and S_2, amplifiers and front end electronics.

The coincidence of two trigger dectors (read out by PMTs) was used to trigger the data acquisition (DAQ program: WaveDump). The high energy particle beam crossed through the middle of the scintillator prototype. The resulting signal from the sensor boards was amplified and transmitted to the waveform digitizer (CAEN DT5742). The raw waveform from each channel was processed as follows (see Fig. 7.2): set amplitude threshold, fit the leading edge and get the time value from the leading edge at half amplitude level [36].

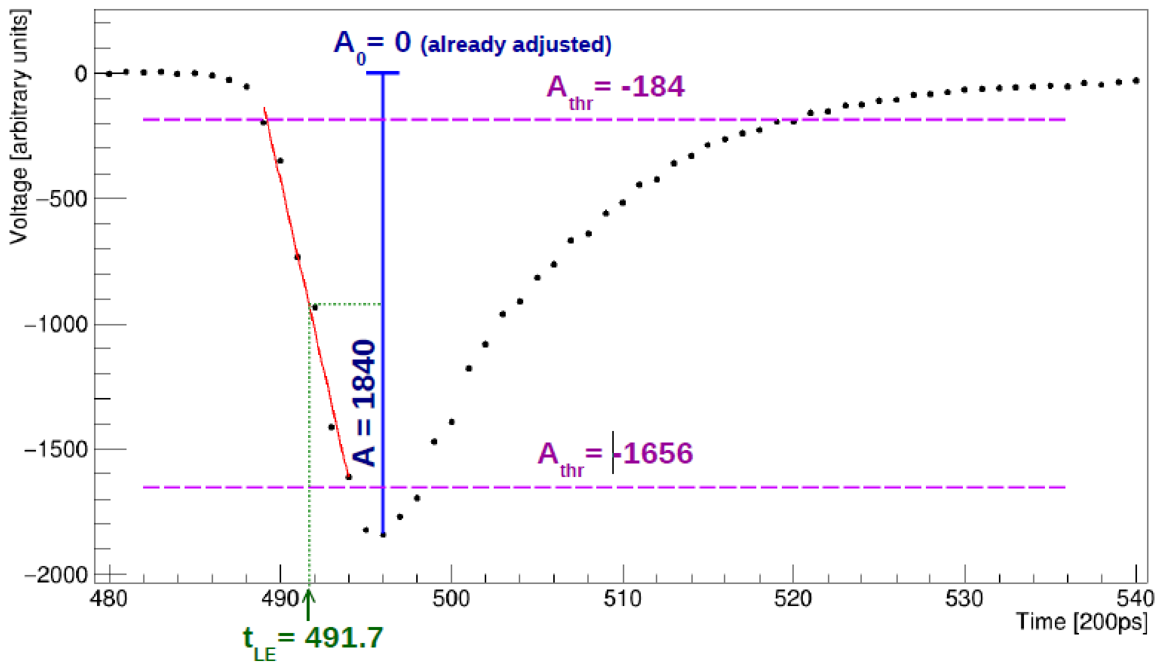

Figure 7.2: Extracting time information from the raw waveform[7], with t_{LE} being the time value.

The bias voltage for each sensor boards was 230 V. The scintillator prototype was positioned in so that the beamline crossed through the middle of the scintillator. The time of flight resolution (tr) was calculated in various ways, as shown in the table 7.2. With the method used in previous chapters (time difference resolution) a time resolution of 114 ps was achieved with the scintillator prototype. The trigger detectors (PMTs) had a time resolution of 25 ps. By calculating the time of flight resolution between the prototype and trigger detector ($\frac{S1+S2}{2} - \frac{T1+T2}{2}$) a value of 70 ps was achieved (see Fig. 7.3).

[7] Maciej Slupecki "FIT tutorial" 2016

Various methods of calculating the time resolution	Time resolution values [ps]
$\frac{S1 - S2}{2}$	114
$S1 - \frac{T1 + T2}{2}$	142
$S2 - \frac{T1 + T2}{2}$	132
$\frac{S1 + S2}{2} - T1$	72
$\frac{S1 + S2}{2} - T2$	71
$\frac{S1 + S2}{2} - \frac{T1 + T2}{2}$	70
$\frac{T1 - T2}{2}$	25

Table 7.1: When calculating the time of flight resolution, a minimum of two channels is needed. Time resolution values are listed for scintillator prototype and (last value) for the trigger detector (two trigger detectors (T1,T2) and the two channels coming from the scintillator prototype (S1,S2)). With the SciTil configuration (scintillator read out on both sides by 4 SiPMs) the "L-R Method" ($\frac{S1-S2}{2}$) is a standard method to evaluate the intrinsic time resolution.

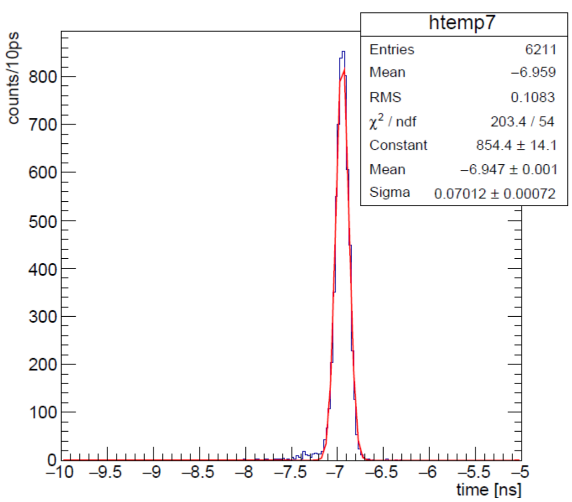

Figure 7.3: Time of flight resolution from 6211 events.

The histogram in Fig. 7.3 was fitted with a gaussian function to extract the time of flight resolution (σ=70 ps). The histograms for the other methods listed in Table 7.1 are attached in the appendices (A.2).

Chapter 8

Summary and outlook

The first day of PANDA physics is planned to start in 2022. In order to reach its maximum potential, the PANDA detector system will need a TOF counter with an excellent time resolution (σ value under 100 ps). The goal of this thesis was to optimize the timing performance of a single scintillator tile.

A decisive step towards an optimal timing in whole TOF counter is to optimize the time resolution of a single tile. Firstly, fast scintillators with optimal properties regarding the signal rise time, decay time and light yield were selected (EJ-228,EJ-232). Since the light generated by scintillators is captured by SiPMs, the quality of these sensors has a great impact on time resolution. The SiPMs should have good electronic and optical properties, as follows: low dark count rate, afterpulses and crosstalk; high detection efficiency and low timing jitter. For this reason, the S13360 series from Hamamatsu is convenient. The next step is to connect the SiPMs in a way that is more suitable for the purpose. Therefore, the serial or hybrid connection of SiPMs is preferred, mainly because it improves the signal rise time and decreases the number of channels. The signal output coming from the SiPMs is usually too low and based on these grounds the use of an voltage amplifier that does not deteriorate the signal rise time is necessary. A first time resolution test with the single tile prototype was done in chapter 5.1.3, where sigma values ($\Delta t_{\mathrm{counter}}$) around 80 ps were achieved. At this point it was clear, that the time resolution could be further improved. One of the limiting factors is definitely the source of high external noise, which could be avoided if the experiment is carried out in a shielded box, which could act as faraday cage.

The time resolution could also depend on the hit position of charged particles on scintillator. Our colleagues from Erlangen Institute have a remotely controlled stepper motor, which could move the source of electrons in x,y direction and therefore the time resolution could be measured across the whole scintillator surface. Under these conditions, the performance of the single tile prototype was optimized. After finding the best applied over-voltage to the SiPMs, electronic threshold and wrapping, a mean time resolution (resulting from 3069 different hit positions on scintillator) of $\Delta t_{counter} = 54$ ps was achieved.

The timing performance of the prototype should be investigated also in an environment that has similar condition as those expected at PANDA. For this reason, a first test was carried out this June with the already optimized prototype at CERN. The single tile prototype was tested under a beam line containing different particle species at 6 GeV energies. A time of flight resolution of 70 ps was achieved.

At this point, the tests with a single tile have come to an end. Further timing tests are currently on-going with the dual-module and super-module. The detector in its final design will use most likely a TOF-PET chip, which will provide bias, signal amplification and electronic threshold for the SiPMs output signal. Colleagues are currently working to adapt this TOF-PET chip to the SiPMs.

List of Figures

List of Tables

List of Abbreviations

ALICE	A Large Ion Collider Experiment
APD	Avalanche Photo Diode
APPA	Atomic Plasma Physics and Applications
CAEN	Costruzioni Apparecchiature Elettroniche Nucleari
CBM	Compressed Baryonic Matter
CERN	Conseil Européen pour la Recherche Nucléaire
DAQ	Data Acquisition
DIRC	Detection of Internally Reflected Cherenkov light
EJ	Eljen
EMC	Electromagnetic Calorimeter
ESR	Enhansed Speculiar Reflector
FAIR	Facility for Antiproton and Ion Reasearch
FS	Forward Spectrometer
GEM	Gas Electron Multiplier
GM	Geiger Müller
GSI	Gesellschaft für Schwerionenforschung
HESR	High Energy Storage Ring
HPK	Hamamatsu Photonics
ISEG	Independent Safety Engineering Group
LINAC	Linear Accelerator
MD	Muon Detection

MPPC	Multi Pixel Photon Counter
MVD	Micro Vertex Detector
NIM	Nuclear Instrumentation Module
NUSTAR	Nuclear structure, Astrophysics and Reactions
PANDA	Antiproton Annihilation in Darmstadt
PCB	Printed Circuit Board
PDE	Photon Detection Efficiency
PET	Positron Emission Tomography
PID	Particle Identification
PMT	Photomultiplier Tube
PSI	Paul Scherrer Institute
PZC	Pole Zero Cancellation
QCD	Quantum Chromodynamics
QDC	Charge-to-Digital Converter
RESR	Accumulator Storage Ring
RICH	Ring Imaging Cherenkov detector.
SciTil	Scintillator Tile
SiPM	Silicon Photomultiplier
SIS100	Super Ion Synchrotron
STT	Straw Tube Tracking system
TDC	Time-to-Digital Converter
TOF	Time Of Flight
TPC	Time Projection Chamber
TS	Target Spectrometer

UNILAC	Universal Linear Accelerator
VME	VERSA Module Eurocard

Appendices

A.1

Scientific activity during my work at Stefan Meyer Institute 01.10.2015-31.10.2016:

Beamtime at CERN, east counter hall T10, 8-16 Oct 2015;

PANDA LV. Collaboration Meeting 30 Nov – 04 Dec, Vienna, Austria;

PANDA LVI. Collaboration Meeting 29 Feb - 04 Mar, Bochum, Germany:

Oral presentation, TOF session: M.Chirita et al. “Status of the SciTil prototype test” 31.03.16

Measurement Erlangen, Germany 16.5.2016 - 20.5.2016

PANDA LVII. Collaboration Meeting 06 Jun - 10 Jun, GSI Darmstadt, Germany:

Oral presentation, TOF session: M.Chirita et al. “Timing performance of a single tile, semifinal results”, 07.06.16

PANDA LVIII. Collaboration Meeting 12 Sep - 16 Sep, Mainz, Germany:

Oral presentation, TOF session: M. Chirita et al.“Timing performance of a single tile, final results”, 13.09.16

66th Yearly Meeting of the Austrian Physical Society ,September 27- 29.16, University of Vienna:

Oral presentation, Marius Constantin Chirita Mihaila et al. “Timing resolution performance of the $\overline{\text{P}}$ANDA SciTil detector using Silicon Photomultiplier (SiPM)” 28.09.16

A.2

Histogram fits for the beamtime measurement (chapter 7).

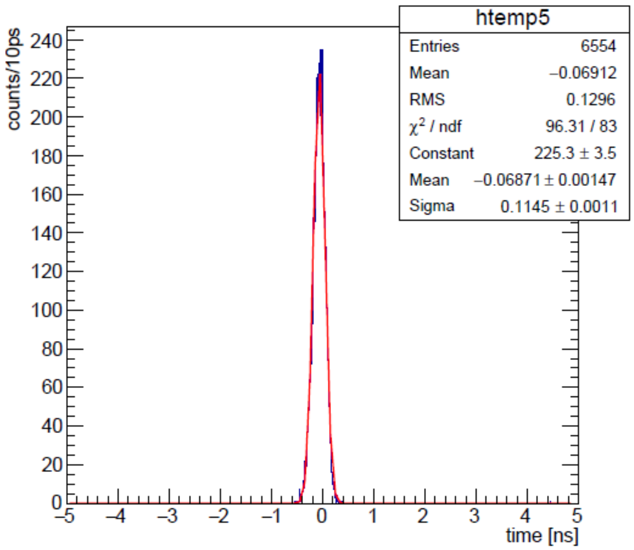

$$\frac{S1 - S2}{2}$$

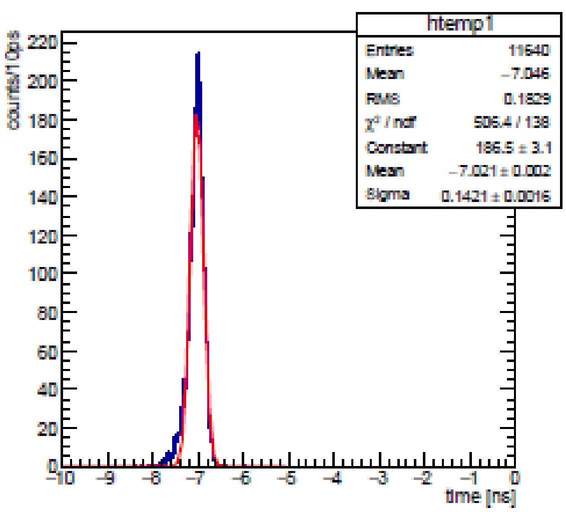

$$S1 - \frac{T1 + T2}{2}$$

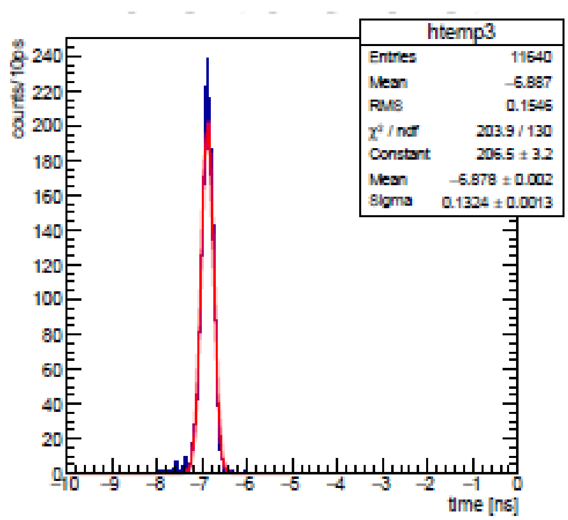

$$S2 - \frac{T1 + T2}{2}$$

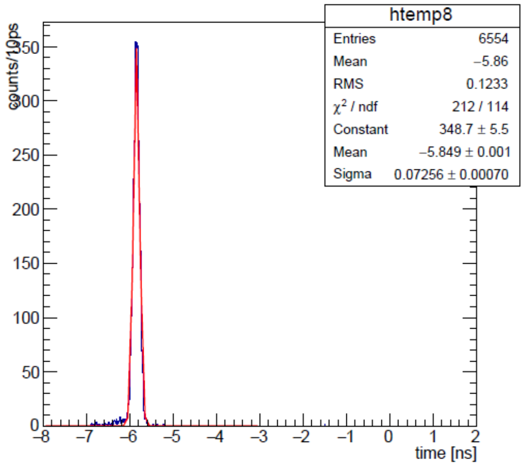

$$\frac{S1+S2}{2}-T1$$

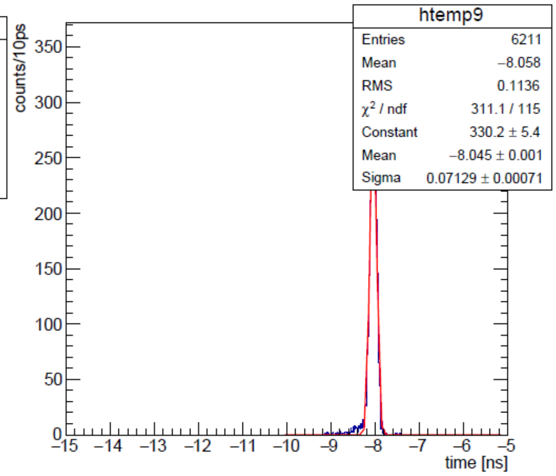

$$\frac{S1+S2}{2}-T2$$

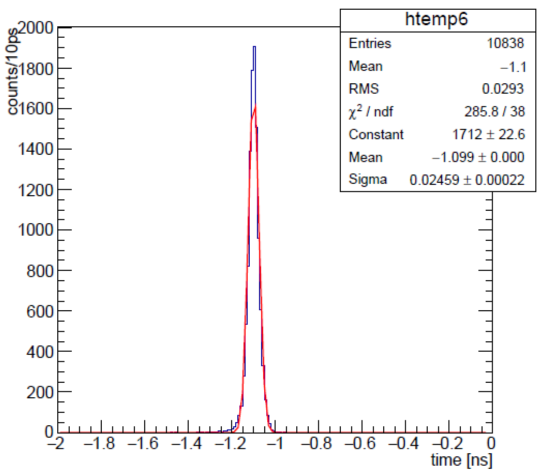

$$\frac{T1-T2}{2}$$

Bibliography

[1] D. Renker "*Geiger-mode avalanche photodiodes, history, properties and problems*", Nucl. Instrum. Meth. A 567 (2006) 48–56.

[2] Stefan Seifert, Member, IEEE, Herman T. van Dam, Ruud Vinke, Member, IEEE, Peter Dendooven, Member, IEEE, Herbert Löhner, Member, IEEE, Freek J. Beekman, Senior Member, IEEE, and Dennis R. Schaart, Member, IEEE. "*A Comprehensive Model to Predict the Timing Resolution of SiPM-Based Scintillation Detectors: Theory and Experimental Validation*" IEEE TRANSACTIONS ON NUCLEAR SCIENCE, VOL. 59, NO. 1, FEBRUARY 2012.

[3] L. Gruber "*Studies of SiPM photosensors for time-of-flight detectors within PANDA at FAIR*", Dissertation, Technische Universitaet Wien (2014), https://imgm.iaea.org/record/349/files/AT1602052.pdf

[4] A. Stoykov, R. Scheuerman, K. Sedlak, "*A time resolution study with a plastic scintillator read out by a Geiger-mode Avalanche Photodiode*", Nucl. Instrum. Meth. A 695 (2012) 202-205.

[5] www.hamamatsu.com/jp/en/S13360-6050PE

[6] Sergei Dolinsky, Geng Fu, Adrian Ivan, "*Timing resolution performance comparison of different SiPM devices*", Nucl. Instrum. Meth. A 801 (2015) 11-20.

[7] Bettoni, D. "*The PANDA Experiment at FAIR*", proceedings of the CHARM 2007 Workshop, Ithaca, NY, August 5-8, 2007, http://www.slac.stanford.edu/econf/C070805/PDF/39_Bettoni.pdf.

[8] Gianluigi Boca on the behalf of the PANDA collaboration, "*The PANDA experiment, physics goals and experimental setup*", EPJ Web of Conferences 72, 00002 (2014).

[9] PANDA Collaboration, "Physics Performance Report for PANDA: Strong Interaction Studies with Antiprotons", (2009) https://arxiv.org/abs/0903.3905.

[10] Dipanwita Dutta for the PANDA Collaboration, "*Physics program of PANDA experiment at FAIR*", Nuclear Physics A 862–863 (2011) 231–237.

[11] Gianluigi Boca ”*PANDA at FAIR :physics goals and experimental overview*” talk, Hirschegg, January 2011, http://theorie.ikp.physik.tu-darmstadt.de/hirschegg/2011_backup/talks/BocaHirschegg11_new.pdf.

[12] C.Schwarz for the PANDA collaboration ”*The PANDA Experiment at FAIR*” Journal of Physics: Conference Series 374 (2012) 012003.

[13] Albrecht Gillitzer on behalf of the PANDA Collaboration, “*Strong interaction* physics *with antiproton-induced reactions at PANDA*”, Hyperfine Interact. (2014) 229:21–29.

[14]P. Hoyer, “*Introduction to QCD - a bound state perspective*”, Arxiv ID: 1106.1420.

[15] K. Suzuki et al., “*Technical Design Report for the :PANDA Barrel Time-of-Flight*” not yet published.

[16] K. Suzuki, “Time Resolution Calculation”, talk at PANDA collaboration meeting, TOF session, GSI, 11.03.2014.

[17] Pouthas, J. ; Agarwal, S. ; Engrand, M. ; Pisani, C, “*Intrinsic time resolution of detectors in a time-of-flight spectrometer*”, Nucl. Instrum. Meth. Vol. 145 (1977) 445-451.

[18] “An Introduction to the Silicon Photomultiplier”, (2011) http://www.sensl.com/downloads/ds/TN%20-%20Intro%20to%20SPM%20Tech.pdf.

[19] Slawomir S. Piatek, Hamamatsu Corporation & New Jersey Institute of Technology “Measuring the Electrical and Optical Properties of an MPPC” Febr. 2014, http://www.hamamatsu.com/eu/en/community/optical_sensors/articles/measuring_characteristics_of_mppc/index.html.

[20] Hans-Christian Schultz-Coulon, “Silicon Photomultipliers and their application in HEP and Medical Imaging”, LHCb Retreat Neckarzimmern, March 2014, http://www.physi.uniheidelberg.de/Forschung/he/LHCb/documents/WorkshopNeckarzMar14/SiPMs.pdf.

[21] Slawomir S. Piatek, Hamamatsu Corporation & New Jersey Institute of Technology “Physics and Operation of an MPPC”, (2014) https://www.hamamatsu.com/us/en/community/optical_sensors/articles/physics_and_operation_of_mppc/index.html.

[22] Hermann Kolanoski, Norbert Wermes, "Teilchendetektoren", Springer-Verlag Berlin Heidelberg (2016).

[23] https://www.hamamatsu.com/resources/pdf/ssd/mppc_kapd9003e.pdf

[24] R. Ben-Michael; M.A. Itzler; B. Nyman, "*Afterpulsing Effects in 1.5 μm Single Photon Avalanche Photodetectors*", Conference Proceedings - Lasers and Electro-Optics Society Annual Meeting-LEOS (2007) pp.783-784.

[25] L. Gruber, S. E. Brunner, J. Marton, K. Suzuki, "Over saturation behavior of SiPMs at high exposure", Nucl. Instrum. Meth. A 737 (2014) pages 11-18.

[26] P.K. Lightfoot, G.J. Barker, K. Mavrokoridis , Y.A. Ramachers , N.J.C. Spooner, "Characterisation of a silicon photomultiplier device for applications in liquid argon based neutrino physics and dark matter searches", Journal of Instrumentation, Volume 3 (2008), http://iopscience.iop.org/article/10.1088/1748-0221/3/10/P10001/pdf.

[27] R. Scheuermann, A. Stoykov, D. Renker, Z. Sadygov, R. Mehtieva, A. Dovlatov V. Zhuk, "Scintillation detectors for operation in high magnetic fields: Recent development based on arrays of avalanche microchannel photodiodes", Nucl. Instrum. Meth. A 581 (2007) 443-446.

[28] Ootani, W. ; Ieki, K. ; Iwamoto, T. ; Kaneko, D. ; Mori, T. ; Nakaura, S. ; Nishimura, M. ; Ogawa, S. ; Sawada, R. ; Shibata, N. ; Uchiyama, Y. ; Yoshida, K. ; Sato, K. ; Yamada, R. "*Development of deep-UV sensitive MPPC for liquid xenon scintillation detector*", Nucl. Instrum. Meth. A 787 (2015) 220-223.

[29] Paolo W. Cattaneo, Matteo De Gerone, Flavio Gatti, Miki Nishimura, Wataru Ootani, Massimo Rossella, and Yusuke Uchiyama, "Development of High Precision Timing Counter Based on Plastic Scintillator with SiPM Readout" IEEE Transactions on Nuclear Science, vol. 61 (2014) 2657-2666.

[30] Daisuke Kaneko on behalf of the MEG collaboration, "Upgrade of the liquid xenon γ-ray detector in the MEG experiment", Nucl. Instrum. Meth. A732 (2013) 457-462.

[31] L. Gruber, M. Chirita, P. Bühler, J. Marton, D. Steinschaden, K. Suzuki, J. Zmeskal, "SciTil new prototype tests", Talk at PANDA collaboration meeting, December 1, 2015.

[32] J. Huizenga; S. Seifert; F. Schreuder; H.T. van Dam; P. Dendooven; H. Löhner; R. Vinke; D.R. Schaart, "*A fast preamplifier concept for SiPM-based time-of-flight PET detectors*", Nucl. Instrum. Meth. A 695 (2012) 379-384.

[33] root, https://root.cern.ch/

[34] Ken Suzuki, "Particle contaminations in the time of flight spectrum and its influence to the time resoluti on measurementat the CERN T10 beam line", talk at (FIT) ALICE meeting, CERN, 18.7.2016.

[35] 3m optical systems ,"Ehanced Specular Relflector (ESR)", http://www.apioptics.com/pdf/ESR.pdf.

[36] Maciej Slupecki "FIT tutorial" talk held before FIT beam test at PS (06.2016) , Vidyo, 30.05.2016.

[37] Sergei Dolinsky, Geng Fu, and Adrian Ivan, "Timing Resolution Performance Comparison for Fast and Standard Outputs of SensL SiPM" IEEE Nuclear Science Symposium and Medical Imaging Conference (2013) print ISSN: 1082-3654.

[38] K. Ieki, " *Upgrade of the MEG liquid xenon calorimeter with VUV-light sensitive large area SiPMs*", Nucl. Instrum. Meth. A 824 (2016) 686-690.

[39] A. Ferri, F. Acerbi, A. Gola, G. Paternoster, C. Piemonte and N. Zorzi, "*Performance of FBK low-afterpulse NUV silicon photomultipliers for PET application*", (2016) JINST, vol. 11, no. 03, pp. P03 023-P03 023.